

Plasma-Enhanced Etching and Deposition

Dennis W. Hess and David B. Graves

Department of Chemical Engineering, University of California, Berkeley,
CA 94720

Chemical and chemical engineering principles involved in plasma-enhanced etching and deposition are reviewed, modeling approaches to describe and predict plasma behavior are indicated, and specific examples of plasma-enhanced etching and deposition of thin-film materials of interest to the fabrication of microelectronic and optical devices are discussed.

THE INCREASING COMPLEXITY OF SOLID-STATE electronic and optical devices places stringent demands upon the control of thin-film processes. For example, as device geometries drop below the 1- μm level, previously standard processing techniques for thin-film etching and deposition become inadequate. For etching, the control of film etch rate, uniformity, and selectivity is no longer sufficient; the establishment of film cross sections or profiles is crucial to achieving overall reliability and high-density circuits. Low-temperature deposition methods are required to minimize defect formation and solid-state diffusion and to be compatible with low-melting-point substrates or films. Therefore, the established techniques of liquid etching and, to some extent, chemical vapor deposition (CVD) are being replaced by plasma-assisted methods. Plasma-assisted etching and plasma-enhanced CVD (PECVD) take advantage of the high-energy electrons present in glow discharges to dissociate and ionize gaseous molecules to form chemically reactive radicals and ions. Because thermal energy is not needed to break chemical bonds, reactions can be promoted at low temperatures (<200 °C).

Although the chemistry and physics of a glow discharge are extraordinarily complex, the plasma performs only two basic functions. First, reactive

0065-2393/89/0221-0377\$15.60/0
© 1989 American Chemical Society

chemical species are generated by electron-impact collisions; thus they overcome kinetic limitations that may exist in thermally activated processes. Second, the discharge supplies energetic radiation (e.g., positive ions, neutral species, metastable species, electrons, and photons) that bombard surfaces immersed in the plasma and thus alter the surface chemistry during etching and deposition. The combination of these physical processes with the strictly chemical reactions due primarily to atoms, radicals, or molecules yields etch rates, etch profiles, and material properties unattainable with either process individually.

Dry Processing

Liquid etching has been the preferred method for pattern delineation for thin films for many years (1). Its pervasive use has been due primarily to two considerations. First, although the exact chemistry is often poorly understood, the technology of liquid etching is firmly established. Second, the selectivity (ratio of film etch rate to the etch rate of the underlying film or substrate) can be essentially infinite with the proper choice of etchant solution.

Despite these advantages, several critical problems arise for micrometer and submicrometer pattern sizes. Resist materials often lose adhesion in the acid solutions used for most etch processes and thereby alter pattern dimensions and prevent line width control. As etching proceeds downward into the film, it proceeds laterally at an approximately equal rate. The mask is undercut, and an isotropic profile (Figure 1) results. Because film thickness and etch rate are often nonuniform across a substrate, overetching is required to ensure complete film removal. Overetching generates a decrease in pattern size because of the continued lateral etching and thus affects process control. When the film thickness is small relative to the minimum pattern dimension, undercutting is insignificant. But when the film thickness is comparable with the pattern size, as is the case for current and future devices, undercutting is intolerable. Finally, as device geometries decrease, spacings between resist stripes also decrease. With micrometer and submicrometer patterns, the surface tension of etch solutions can cause the liquid to bridge the space between resist stripes. Because the etch solution does not contact the film, etching is precluded.

The limitations encountered with solution etching can be overcome by plasma-enhanced etching. Adhesion is not a major problem with dry-etch methods. Undercutting can be controlled by varying the plasma chemistry, gas pressure, and electrode potentials (2–6) and thereby generate directional or anisotropic profiles.

Numerous techniques have been developed for the formation of thin-film materials (7–9). Because of the versatility and throughput capability of CVD, this method has gained wide acceptance for a variety of film materials.

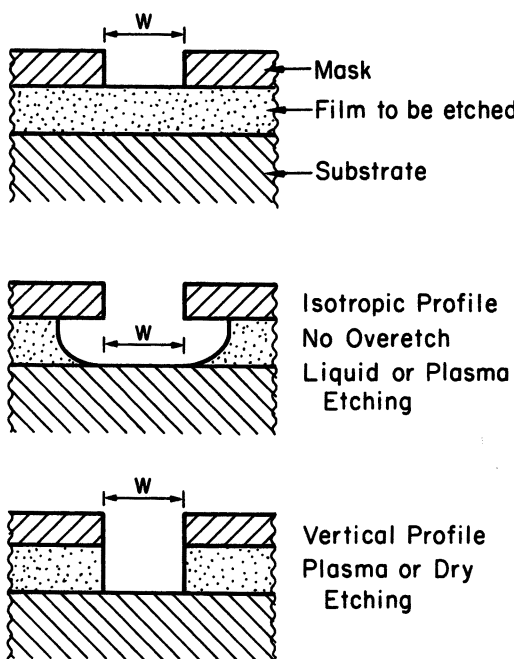


Figure 1. Cross sections of films etched with liquid or plasma etchants. The isotropic profile is the result of zero overetch and can be generated with liquid or plasma etch techniques. The anisotropic (vertical) profile requires plasma or dry-etch processes. W is the width of the resist pattern. (Reproduced from reference 2. Copyright 1983 American Chemical Society.)

However, deposition rates are often low with CVD, and the presence of temperature-sensitive substrates or films (e.g., polymers or low-melting-point metals) prior to deposition, along with the possibility of generating defects (e.g., vacancies, interstitials, stacking faults, and dislocations) often precludes the use of elevated temperatures ($>300\text{ }^{\circ}\text{C}$) for film growth. In such cases, deposition rates can be enhanced by using high-energy electrons in a discharge rather than thermal means to supply the energy for bond breaking (10–14).

rf Glow Discharges

The rf (radio frequency) glow discharges (2) or plasmas used for plasma etching or PECVD are partially ionized gases composed of ions, electrons, and a host of neutral species in both ground and excited states. Typically, the plasma is formed by applying an electric field across a volume of gas. Many types of plasmas exist (15); they differ primarily in electron concentration n_e and average electron energy kT_e . A quantity that is useful in

characterizing the average electron energy is the ratio of the electric field to the pressure, E/p (15). As the electric field strength increases, free electrons, whose velocities increase because of acceleration by the field, gain energy. The electrons lose this energy by inelastic collisions, so that an increase in pressure, which decreases the electron mean free path, decreases the electron energy.

In thin-film processes for the fabrication of electronic materials and devices, rf glow discharges are primarily used. The application of an rf voltage at frequencies between 50 kHz and 40 MHz to a low-pressure (6–600 Pa) gas results in a chemically unique environment (Table I.).

Electron densities (n_e) and, because the plasma is electrically neutral, positive-ion densities (n_i) range from 10^8 to $10^{12}/\text{cm}^3$. However, the ratio of the neutral-species density (n_N) to the electron density is usually greater than 10^3 , so that these plasmas are only weakly ionized. As a result, radicals and molecules in the discharge are primarily responsible for etching and deposition reactions. That is, radicals and molecules are not inherently more reactive than ions, but they are present in significantly higher concentrations. The glow discharges described by Table I are termed nonequilibrium plasmas, because the average electron energy (kT_e) is considerably higher than the ion energy (kT_i). Therefore, the discharge cannot be described adequately by a single temperature.

Physical and Electrical Characteristics. The electrical potentials established in the reaction chamber determine the energy of ions and electrons striking the surfaces immersed in a discharge. Etching and deposition of thin films are usually performed in a capacitively coupled parallel-plate rf reactor (see Plasma Reactors). Therefore, the following discussion will be directed toward this configuration.

The important potentials in rf glow discharge systems (16, 17) are the plasma potential (potential of the glow region), the floating potential (potential assumed by a surface within the plasma that is not externally biased or grounded and thus draws no net current), and the potential of the powered or externally biased electrode. When the plasma contacts a surface, that surface, even if grounded, is usually at a negative potential with respect to the plasma (16, 18, 19). Therefore, positive-ion bombardment occurs. The energy of the bombarding ions is established by the difference in potential

Table I. Properties of rf Glow Discharges (Plasmas) Used for Thin-Film Etching and Deposition

Parameter	Value
$n_e = n_i$	$10^8\text{--}10^{12}/\text{cm}^3$
n_N	$\sim 10^{15}\text{--}10^{16}/\text{cm}^3$
kT_e	1–10 eV
kT_i	~ 0.04 eV

between the plasma and the surface that the ion strikes, the rf frequency (because of mobility considerations), and the gas pressure (because of collisions). Because ion energies may range from a few volts to more than 500 V, surface bonds can be broken, and in certain instances, sputtering of film or electrode material may occur (16).

The reason for the different potentials within a plasma system becomes obvious when electron and ion mobilities are considered (19a). Imagine applying an rf field between two plates (electrodes) positioned within a low-pressure gas. On the first half-cycle of the field, one electrode is negative and attracts positive ions; the other electrode is positive and attracts electrons. Because of the frequencies used and because the mobility of electrons is considerably greater than that of positive ions, the flux (current) of electrons is much larger than that of positive ions. This situation causes a depletion of electrons in the plasma and results in a positive plasma potential.

On the second half-cycle, a large flux of electrons flows to the electrode that previously received the small flux of ions. Because plasma-etching systems generally have a dielectric coating on the electrodes or a series (blocking) capacitor between the power supply and the electrode, no direct current (dc) can be passed. Therefore, on each subsequent half-cycle, negative charge continues to build on the electrodes and on other surfaces in contact with the plasma, and so electrons are repelled and positive ions are attracted to the surface. This transient situation ceases when a sufficient negative bias is achieved on the electrodes such that the fluxes of electrons and positive ions striking these surfaces are equal. At this point, time-average (positive) plasma and (negative) electrode potentials are established.

A plasma potential that is positive with respect to electrode potentials is primarily a consequence of the greater mobility of electrons compared with positive ions. When there are many more negative ions than electrons in the plasma (e.g., in highly electronegative gases), plasma potentials are below electrode potentials, at least during part of the rf cycle (19b).

The plasma potential is nearly uniform throughout the observed glow volume in an rf discharge, although a small electric field directed from the discharge toward the edge of the glow region exists. Between the glow and the electrode is a narrow region (typically 0.01–1 cm, depending primarily upon pressure, power, and frequency) wherein a change from the plasma potential to the electrode potential occurs. This region is called a sheath or dark space and can be likened to a depletion layer in a semiconductor device in that most of the voltage is dropped across this region.

Positive ions drift to the sheath edge where they encounter the strong field. The ions are then accelerated across the potential drop and strike the electrode or substrate surface. Because of the series capacitor or the dielectric coating of the electrodes, the negative potentials established on the two electrodes in a plasma system may not be the same. For instance, the ratio of the voltages on the electrodes depends upon the relative electrode areas

(20). The theoretical dependence is given by equation 1, where V is the voltage and A is the electrode area (20).

$$V_1/V_2 = (A_2/A_1)^4 \quad (1)$$

If V_1 is the voltage on the powered electrode and V_2 is the voltage on the grounded electrode, then the voltage ratio is the inverse ratio of the electrode areas raised to the fourth power. However, for typical etch systems, the exponent of the area ratio is generally less than 4 and may be less than 1.2 (16). This apparent deviation from theory is in part due to the reactor configuration. Although the physical electrodes in a plasma reactor often have the same area, A_2 represents the grounded electrode area, that is, the area of all grounded surfaces in contact with the plasma. Because this area usually includes the chamber walls, the area ratio can be quite large. Because of such considerations, the average potential distribution in a typical commercial plasma reactor with two parallel electrodes immersed in the plasma is similar to that shown in Figure 2 (16). In this case, the energy of ions striking the powered electrode or substrates on this electrode will be higher than that of ions reaching the grounded electrode. Indeed, equation 1 can be used to design electrode areas for reactors such that a particular voltage can be established on an electrode surface.

In addition to the ratio of electrode areas, other plasma parameters can

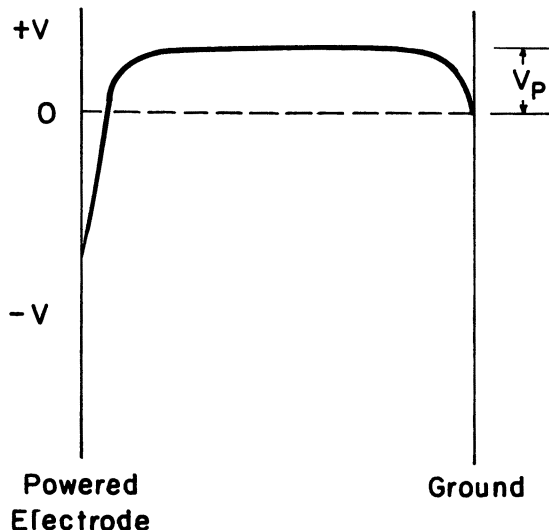


Figure 2. Potential distribution in a parallel-plate plasma etcher with the grounded surface area larger than the powered electrode area. V is the potential, and V_p is the plasma potential. (Reproduced with permission from reference 16. Copyright 1979 The Electrochemical Society, Inc.)

affect the electrical characteristics of the discharge. Varying the rf power input will alter plasma and electrode potentials, as well as ion concentrations, and thereby change ion energies and fluxes. Also, radio frequency affects the kinetic energy of ions that strike surfaces in contact with the plasma. This effect can be readily understood by considering the behavior of an ion experiencing an oscillating plasma potential caused by applied rf voltages (21, 22). Depending upon the ion mobility, some frequency exists above which the ion can no longer follow the alternating voltage. Therefore, the ion cannot traverse the sheath in one half-cycle. Above this frequency, ions experience an accelerating field (the difference between the plasma and electrode potentials divided by the sheath thickness) that is an average over a number of half-cycles. At lower frequencies, where the ions can respond directly to the oscillating field, they are accelerated by instantaneous fields. Thus, the ions can attain the maximum energy corresponding to the maximum instantaneous field across the sheath. As a result, for a constant sheath potential, ion bombardment energies and fluxes are higher at lower frequencies.

Chemical Characteristics. Because etching or deposition processes are merely chemical reactions that yield a volatile or involatile product, respectively, the overall process can be broken down into the following six primary steps:

1. Generation of reactive species
2. Diffusion to the surface
3. Adsorption
4. Reaction
5. Desorption of volatile products
6. Diffusion of volatile products away from the surface

First, reactive atoms, molecules, and ions must be generated by electron–molecule collisions. Because most of the reactant gases or vapors used for plasma-enhanced etching and deposition do not spontaneously undergo reaction at the low temperatures involved, radicals or atoms must be formed so that heterogeneous chemical reactions can proceed at reasonable rates. The reactive species thus generated diffuse to surfaces where they can adsorb onto a surface site. Sticking coefficients are believed to be large for free radicals, such that chemisorption and surface reactions occur readily (23). Surface diffusion of physically adsorbed species or volatile product molecules can occur.

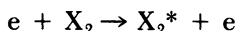
The nature of the primary reaction product differentiates plasma-enhanced etching from deposition. In etching, the volatility of reaction products

is crucial to film removal. Although the principal reaction product in deposition processes is not volatile, secondary products (e.g., hydrogen or halide molecules) must desorb to avoid incorporation into, and thus contamination of, the growing film. Complete elimination of such contamination is difficult, because particle bombardment of adsorbed species can assist incorporation.

As indicated previously, the chemical reactions taking place in glow discharges are exceedingly complex. However, two general types of chemical processes can be categorized: homogeneous gas-phase collisions and heterogeneous surface interactions. To completely understand and characterize plasma processes, the fundamental principles of both processes must be understood.

Homogeneous Processes. Homogeneous gas-phase collisions generate reactive free radicals, metastable species, and ions. Therefore, chemical dissociation and ionization are independent of the thermodynamic temperature. Electron impact can result in a number of different reactions depending upon the electron energy. The following list indicates these reaction types in order of increasing energy requirement (24–26).

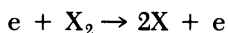
- Excitation (rotational, vibrational, or electronic)



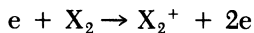
- Dissociative attachment



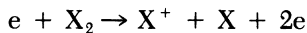
- Dissociation



- Ionization



- Dissociative ionization



Excitation and dissociation processes can occur with mean electron energies below a few electronvolts. Thus, the discharge is extremely effective in producing large quantities of free radicals. Many of these species are generated by direct dissociation, although if attachment of an electron to a molecule results in the formation of a repulsive excited state, the molecule can dissociate by dissociative attachment. These attachment processes are prevalent at low electron energies (<1 eV) when electronegative gases or vapors are used. By comparison, the ionization of many molecules or atoms requires energies greater than ~8 eV, so that relatively few ions exist. The generation of reactive species is balanced by losses due to recombination processes at surfaces (electrodes and chamber walls) and in the gas phase, along with diffusion out of the plasma.

Electron-impact reactions occur at a rate (R) determined by the concentrations of both electrons (n_e) and a particular reactant (N) species (24).

$$R = kn_e N \quad (2)$$

The proportionality constant k is the rate coefficient, which can be expressed by

$$k = \int_{E_{\text{thres}}}^{\infty} (2\epsilon/m)\sigma(\epsilon)f(\epsilon)d\epsilon \quad (3)$$

where ϵ and m are the impinging electron energy and mass, respectively; $\sigma(\epsilon)$ is the cross section for the specific reaction; and $f(\epsilon)$ is the electron energy distribution function. The limits of the integral run from the threshold energy for the impact reaction to infinity. If an accurate expression for $f(\epsilon)$ and electron collision cross sections for the various gas-phase species present are known, k can be calculated. Unfortunately, such information is generally unavailable for many of the molecules used in plasma etching and deposition.

Because of the highly nonequilibrium conditions experienced by electrons in the plasma, $f(\epsilon)$ almost never follows the Maxwell–Boltzmann distribution. In general, the distribution function is determined by the electric field that accelerates electrons and collisions that cause electrons to change energy. Very few direct measurements of $f(\epsilon)$ have been made under conditions of interest to plasma etching or deposition; consequently, the current understanding of $f(\epsilon)$ is limited, at best. This fact impedes the ability to make quantitative predictions of electron-impact rates. As previously described, ionization due to electron impact occurs through the action of the most energetic electrons in the distribution. The number of electrons in the high-energy tail of the distribution that are capable of ionizing neutral species in the discharge is considerably less than the number of electrons capable of molecular dissociation. As a result, the degree of ionization is usually much less than the degree of molecular dissociation.

A second type of homogeneous impact reaction is that occurring between the various heavy species generated by electron collisions, as well as between these species and unreacted gas-phase molecules (27, 28). Again, dissociation and ionization processes occur, but in addition, recombination and molecular rearrangements are prevalent. Particularly important inelastic collisions are those called Penning processes (29). In these collisions, metastable species (species in excited states where quantum mechanical selection rules forbid transition to the ground state and thus have long lifetimes) collide with neutral species, transfer their excess energy, and thereby cause dissociation or ionization. These processes are particularly important with gases, such as argon and helium, that have available a number of long-lifetime metastable states. Furthermore, Penning ionization has a large cross section, which enhances the probability of this process.

Heterogeneous Processes. A variety of heterogeneous processes can occur at solid surfaces exposed to a glow discharge (28, 30–32). The primary processes of interest in plasma etching and deposition are summarized in the following list (23). These interactions result from the bombardment of surfaces by particles.

- Ion–surface interactions
 1. Neutralization and secondary electron emission
 2. Sputtering
 3. Ion-induced chemistry
- Electron–surface interactions
 1. Secondary electron emission
 2. Electron-induced chemistry
- Radical– or atom–surface interactions
 1. Surface etching
 2. Film deposition

Although vacuum-UV photons and soft X-rays present in the plasma are sufficiently energetic to break chemical bonds, electron and, particularly, ion bombardments are the most effective methods of promoting surface reactions (33).

Several theoretical investigations (23, 34, 35) indicate that nearly all incident ions will be neutralized within a few atomic radii of a surface, presumably because of electrons arising from Auger emission processes. These results suggest that the particles ultimately striking surfaces in contact with a glow discharge are neutral species rather than ions. To a first approximation, effects due to energetic ions and neutral species should be similar, provided that the particle energies are the same.

Auger emission to neutralize incoming ions leaves the solid surface in an excited state; relaxation of the surface results in secondary electron generation (23, 24). Secondary electrons are ejected when high-energy ions, electrons, or neutral species strike the solid surface. These electrons enhance the electron density in the plasma and can alter the plasma chemistry near a solid surface. Radiation impingement on a surface can induce a number of phenomena that depend upon the bombardment flux and energy.

As noted previously (33), positive ions (or fast neutral species) are extremely efficient in enhancing surface processes; thus this chapter will concentrate on ion bombardment effects. The various surface, thin-film, and bulk phenomena affected by bombarding species are indicated in Figure 3 (36). The specific processes taking place are designated above the labeled abscissa in Figure 3, along with the range of particle energies that cause such effects.

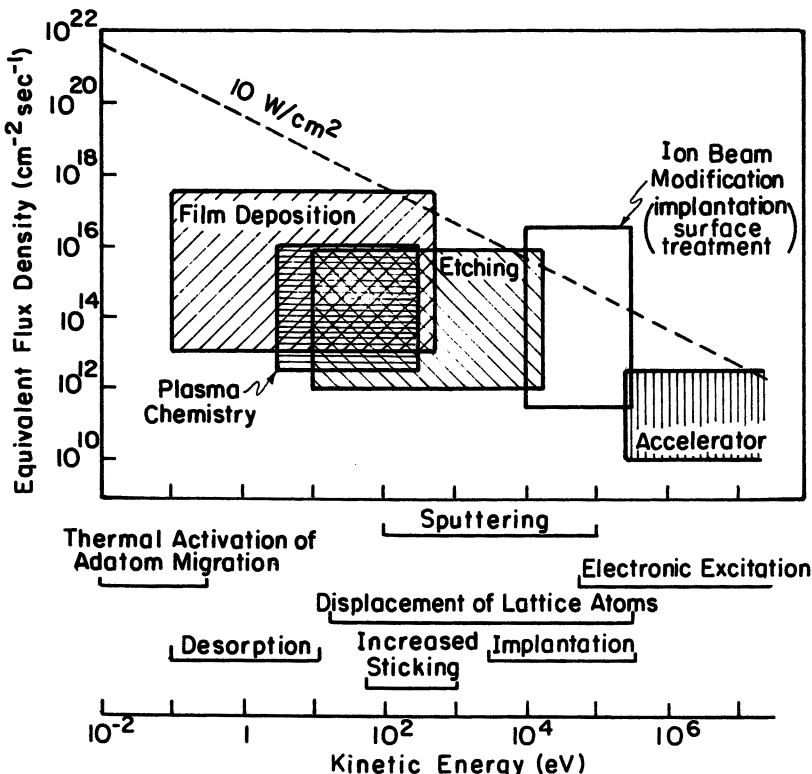


Figure 3. Ranges of kinetic energy and equivalent flux density of incident species for various engineering applications for ion-surface and gas-surface interactions. Kinetic energy ranges of particles in which significant interactions occur are also shown. (Reproduced with permission from reference 36. Copyright 1984 American Institute of Physics.)

Synergistic Phenomena. The enhancement of etch rates and the alteration of deposited film properties due to particle bombardment are well-known phenomena whose generic origins can be simply envisioned by referring to the process steps listed on page 383. Steps 3–5 are heterogeneous processes whose kinetics are temperature dependent. However, temperature is merely one method of increasing the energy of surface bonds. Particle bombardment is another means of imparting energy to a surface. Specifically, ion (or electron) bombardment can break surface bonds and thereby create crystal damage and adsorption sites (37), as well as assist product desorption (38). Also, chemical reactions on the solid surface can be promoted by such bombardment (33). Which of these steps is primarily responsible for enhanced etch rates and film property alteration is not yet clear. Nevertheless, particle bombardment obviously promotes etch processes, as demonstrated by the beam experiments described by Figure 4.

In this study (39), a beam of XeF_2 molecules and a beam of argon ions

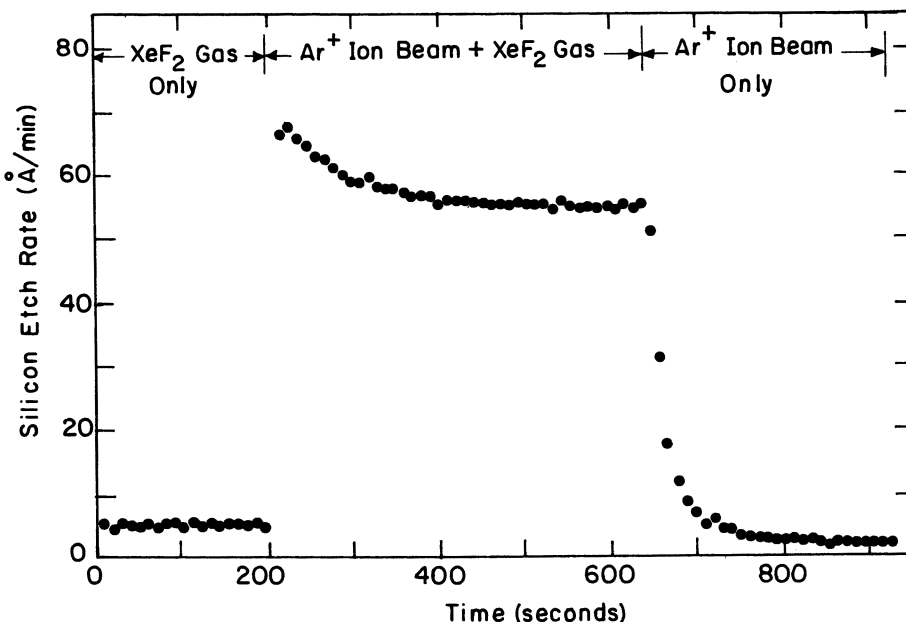


Figure 4. Example of ion-assisted gas-surface chemistry in the etching of silicon with XeF_2 . The XeF_2 flow is $2 \times 10^{15} \text{ mol/s}$, and the argon energy and current are 450 eV and 2.5 μA , respectively. (Reproduced with permission from reference 39. Copyright 1979 American Institute of Physics.)

were directed at a silicon film. Xenon difluoride was used because it afforded a method of depositing fluorine atoms onto the silicon surface. Measurement of the silicon etch rate as a function of XeF_2 or Ar^+ exposure allowed a comparison of chemical and physical etch processes. When only XeF_2 contacted the silicon surface, a small ($\sim 5 \text{ \AA/min}$) purely chemical etch reaction was observed. Likewise, when Ar^+ impinged on the surface, pure sputtering ($\sim 2 \text{ \AA/min}$) was noted. However, when the beams were simultaneously directed at the silicon surface, a relatively large etch rate ($\sim 55 \text{ \AA/min}$) was observed; the measured rate was approximately an order of magnitude greater than the sum of the chemical and physical components. Therefore, synergistic effects due to ion bombardment are crucial to this chemical etch process. However, the exact nature of these effects is at present not well understood. Regardless of the precise cause, particle-bombardment-induced chemistry clearly results in directional etching by promoting higher etch rates in the vertical direction (where ions strike) compared with the lateral direction.

Synergistic phenomena similar to those described for etching are expected during film formation processes. In particular, the creation of adsorption and nucleation sites, along with the promotion of chemical reactions and the dissociation of adsorbed species because of particle bombardment,

should be prevalent with particle energies above 20 eV. However, the various effects of ion bombardment (Figure 3) on the primary processes occurring during growth are extremely difficult to separate (32). Furthermore, although the basic plasma chemistry, physics, and synergistic effects for both etching and deposition are analogous, PECVD introduces one additional complication: Film bonding configurations must be controlled if films with specified and reproducible properties are to be formed.

The previous discussions indicate that a fundamental understanding of gas-phase plasma chemistry and physics, along with surface chemistry modified by radiation effects, is needed in order to define film etch and growth mechanisms. These phenomena ultimately establish etch rates and profiles, as well as film deposition rates and properties. The complex interactions involved in PECVD are outlined in Figure 5 (14, 40). If the basic or microscopic plasma parameters (neutral-species, ion, and electron densities; electron energy distribution; and residence time) can be controlled, the gas-phase chemistry can be defined. Many macroscopic plasma variables (gas flow, discharge gas, pumping speed, rf power, frequency, etc.) can be changed to alter the basic plasma conditions. However, the precise manner in which a change in any of these variables affects basic plasma parameters is currently unknown.

The variation of a macroscopic variable usually results in a change in two or more basic gas-phase parameters, as well as surface potential, particle flux, and surface temperature. For instance, rf power determines the current and voltage between the electrodes in a parallel-plate plasma reactor. Varying the rf frequency changes the number and energy of ions (because of mobility considerations) that can follow the alternating field; thus, bombardment flux and energy are affected. The gas flow rate, the pump speed, and the pressure are interrelated, and two ways of changing the gas pressure can be envisioned. The gas flow rate can be varied at constant pump speed, or the pump speed can be varied (by throttling the pump) at constant gas flow rate. These two methods of pressure variation yield different residence times for the chemical species in the reactor, so that the precise chemistry is altered.

The particular reactant gas and the surface temperature (not necessarily equal to the electrode temperature) are critical parameters because of the dependence of the process on the type and concentration of reactive species and because of the observation that most deposition and etching processes follow an Arrhenius rate expression. Electrode and chamber materials can alter the chemistry occurring in glow discharges because of chemical reactions (adsorption, recombination, etc.) on or with the surfaces. Electrode potential and reactor configuration (equation 1) determine the energy of ions and electrons that strike the surfaces in contact with the discharge. Synergism between these numerous processes results in specific film growth (and etch) mechanisms. Ultimately, these factors establish film composition, bonding structure, and thus film properties.

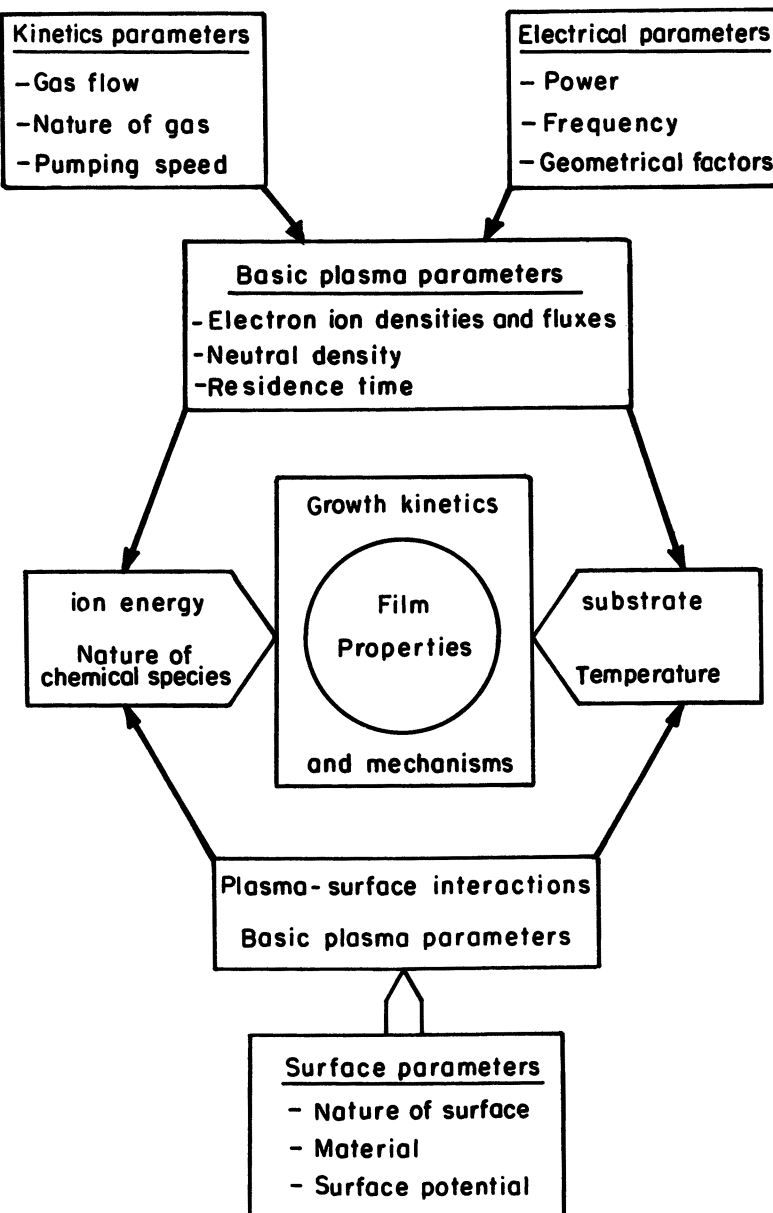


Figure 5. Interaction complexity of homogeneous and heterogeneous plasma processes that determine film properties in PECVD. (Reproduced with permission from reference 14. Copyright 1985 The Electrochemical Society, Inc.)

Radiation Damage. The particle bombardment that occurs during plasma-enhanced film etching and deposition is responsible for etch directionality and for the alteration of film properties. However, if the particle (primarily ion) energies or fluxes are sufficiently high, damage can be created in existing films or substrates. The displacement of atoms generates vacancies, interstitials, dislocation loops, and stacking faults. Even at relatively low bombardment energies, incorporation of light ions can occur, which results in crystal damage.

Considerable efforts have been expended recently to characterize the damage incurred during plasma-enhanced etching (41–44). These studies indicate that dislocation loops and impurity incorporation in substrate materials and films exposed to the plasma are prevalent. Furthermore, the damage can extend to more than 30 nm into substrates even at fairly low ion energies (~ 450 eV). An example of these effects for the case of $\text{CF}_4\text{-H}_2$ etching of SiO_2 on a silicon substrate is shown in Figure 6, for which X-ray photoelectron spectroscopy (XPS), hydrogen depth profiling, and Rutherford

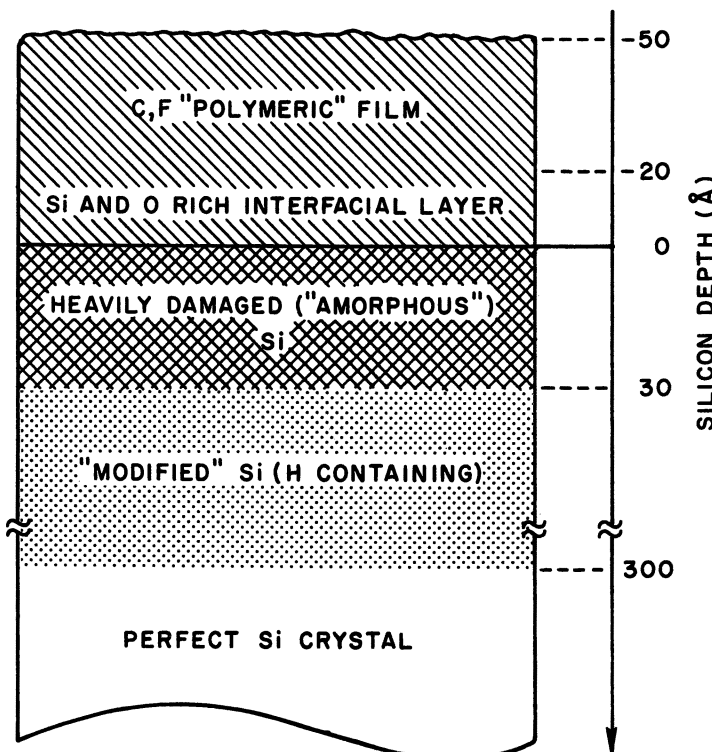


Figure 6. Schematic diagram of changes in silicon near-surface region caused by $\text{CF}_4\text{-H}_2$ reactive-ion etching. (Reproduced with permission from reference 43. Copyright 1985 The Electrochemical Society, Inc.)

back-scattering spectrometry (RBS) were used to characterize the carbonaceous residue and silicon surface region (43). Such damage degrades material properties and alters the characteristics of fabricated devices. In addition, charge formation and accumulation in insulators subjected to radiation during plasma etching can lower the dielectric breakdown strength of device structures (44).

Few studies have been reported that address radiation damage in PECVD processes. Recent work comparing sputter deposition and PECVD for dielectric film deposition indicates that structural damage is minimal in PECVD, although substrate damage is noted for sputtered coatings (45). These differences are probably due to lower ion energies resulting from the higher pressures and lower power densities used in PECVD compared with sputter deposition. Also, substrate temperatures above 200 °C are generally used in PECVD, so that any damage incurred may be annealed during deposition. Finally, in plasma etching, the underlying film or substrate is exposed to the discharge at the end of the etch cycle. With PECVD, underlying surfaces are only briefly exposed at the start of the deposition cycle.

Plasma Reactors

Like CVD units, plasma etching and deposition systems are simply chemical reactors. Therefore, flow rates and flow patterns of reactant vapors, along with substrate or film temperature, must be precisely controlled to achieve uniform etching and deposition. The prediction of etch and deposition rates and uniformity require a detailed understanding of thermodynamics, kinetics, fluid flow, and mass-transport phenomena for the appropriate reactions and reactor designs.

For the most part, plasma-enhanced etching and deposition are performed in four basic reactor types (Figure 7; 2, 46). Each reactor has several basic components: a vacuum chamber and pumping system to maintain reduced pressures, a power supply to create the discharge, and gas- or vapor-handling capabilities to meter and control the flow of reactants and products.

Barrel Reactor. Chronologically, the first and still the simplest etching system is the barrel reactor. This configuration generally uses a cylindrical chamber with rf power applied to external coils or external electrodes. Substrates are placed in a holder or “boat” within the chamber. To improve temperature uniformity along the length of the holder and to minimize particle bombardment of substrates, a perforated cylindrical “etch tunnel” is often inserted in the reactor. This metal cylinder acts as a Faraday cage and confines the glow region to the annulus between the etch tunnel and the chamber wall. Substrates are thereby shielded from the plasma and are subjected to little, if any, ion or electron bombardment. However, neutral species diffuse through the perforations and reach film surfaces. In this case,

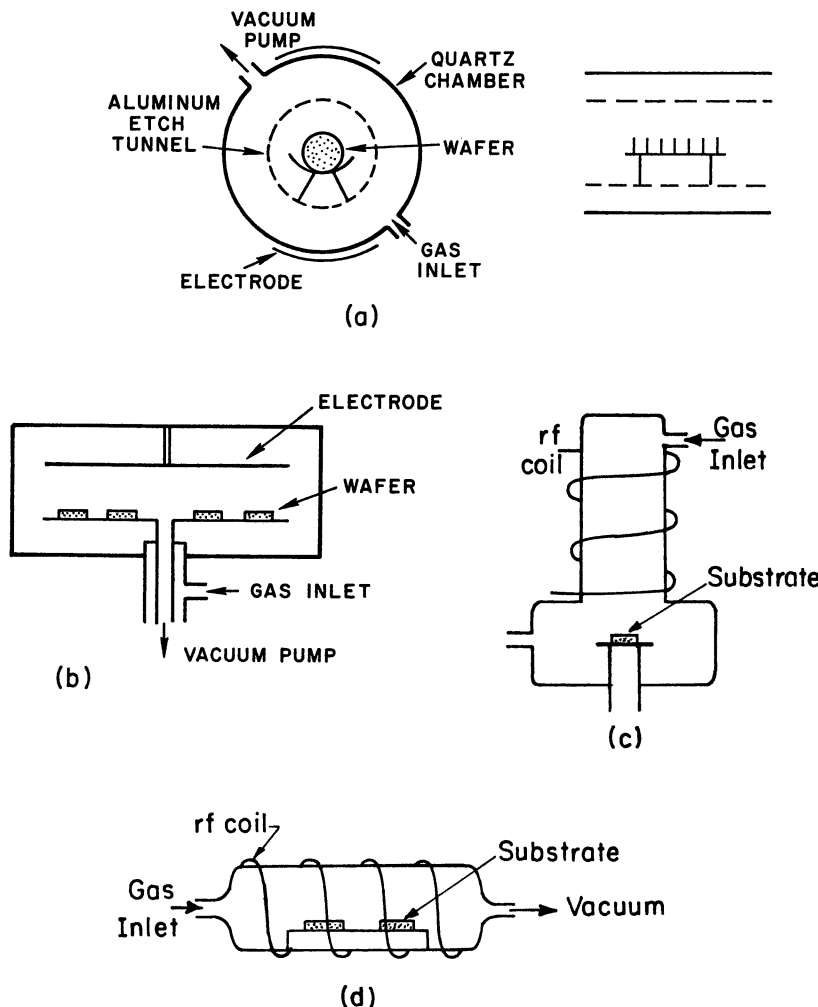


Figure 7. Configuration for plasma etch and deposition reactors. (a) parallel-plate or surface-loaded design with wafers positioned horizontally; (b) parallel-plate design with vertical electrodes with a furnace tube; (c) external coupling, downstream; (d) external coupling. (a: Reproduced from reference 2. Copyright 1983 American Chemical Society. b-d: Reproduced with permission from reference 46. Copyright 1983 American Society for Testing and Materials.)

the etch reaction is almost purely chemical (like liquid etching) and results in an isotropic etch profile. Therefore, barrel systems are usually used for resist stripping or in noncritical etching steps where undercutting can be tolerated.

Planar or Parallel-Plate Reactor. Because very-large-scale integration (VLSI) demands nearly vertical etch profiles, planar or parallel-plate

reactors are favored for many etch processes. In this configuration (Figure 7a), which is similar to that used in rf sputtering, the substrates lie on an electrode within the plasma. The substrates are subjected to energetic radiation that imparts both physical and chemical components to the etch (or deposition) process. The physical component can induce directionality during film etching and can alter the properties of the deposited film by promoting surface reaction steps.

In PECVD, substrates are placed on the grounded electrode, and the opposite electrode is powered. Etching that is performed in this mode is generally called plasma etching. However, when substrates are positioned on the powered electrode for etching purposes, a reactive-ion-etching (RIE) or reactive-sputter-etching configuration results (38, 47, 48). The RIE arrangement generally causes the wafers to be subjected to higher energy ion bombardment than does the plasma-etching mode because of the potentials established on the grounded electrode versus the powered electrode (*see* Physical and Electrical Characteristics of rf Glow Discharges). Another reason for higher energy ions in RIE is the lower operating pressure. No exact pressure demarcation exists; however, RIE is typically carried out at pressures below 13 Pa, whereas plasma etching is performed at higher pressures.

When parallel-plate reactors are used for PECVD, substrates can be positioned horizontally or vertically (Figure 7b). The vertical position is often used to enhance throughput. PECVD processes are usually performed at electrode temperatures below 400 °C. If higher temperatures are desired (e.g., for epitaxial deposition), inductive coupling using external coils is often invoked to eliminate problems of film contamination arising from the electrode material. In this approach, the substrates may be positioned outside of (Figure 7c) or within (Figure 7d) the plasma volume.

The “downstream” configuration (Figure 7c) is particularly interesting because of its flexibility in controlling or modifying the specific chemistry that occurs (49, 50). All feed gases can be passed through the discharge, and the fragments can be allowed to react at the heated (or cooled) substrate surface. Alternatively, one (or more) of the reactants (or diluents) can be excited or dissociated by the plasma, and the reactive fragments can be brought into contact with other reactant molecules at the substrate surface. In this way, specific chemical bonds can be broken or specific molecules can be excited, and improved discrimination may result in the reaction chemistry and thus in the film-bonding structure.

Finally, downstream configurations are also used for etching processes. In these applications, problems of temperature control and radiation damage (bond breaking because of radiation impingement on solid surfaces) are minimized or eliminated. To enhance the etch rate, microwave radiation has been used to generate long-lived chemical species that are then transported

to the wafers (51, 52). Such approaches often permit independent control of ion flux and energy to etching surfaces.

Modeling Plasma Processes

Modeling Requirements. To understand plasma processes in a systematic and comprehensive way, a mathematical model is useful. Because of the enormous complexity of chemically reacting plasmas, the relationships between different physical and chemical processes in the discharge are difficult to quantify and, sometimes, even to identify. To date, only a few preliminary attempts to model discharges in any detail have been made. Even for chemically inert gases, few efforts have been made to model the complete discharge (sheath-and-glow) region. Much of the modeling work has addressed the positive column of a direct-current (dc) discharge in a cylindrical tube. The positive column has received more attention because of its importance in gas discharge lighting and gas discharge lasers and also, undoubtedly, because of the relative simplicity of the analysis for this region. Under the proper conditions, the properties of the positive column vary only slightly in the axial direction, and therefore, discharge properties are assumed to vary only in the radial direction. A comprehensive review of the state of the art in modeling the positive column is available (53).

Discharge Behavior. A chemical reactor model of discharge behavior must take into account both discharge physics and discharge chemistry. Discharge physics includes the charged-particle densities and energies and the electric field strength. These quantities are important in creating chemically active radicals (primarily through electron-impact dissociation of reactants) and in influencing surface reactions (mainly through ion bombardment). Discharge chemistry includes gas-phase and surface reactions between ion and neutral species, as well as the transport of these species by convection and diffusion. Plasma reactors are generally not isothermal, although temperature gradients in plasma reactors are relatively small compared with those in CVD. As a result, an energy balance must be solved in order to determine the temperatures in the system.

The physical structure of a discharge is complicated by the fact that the discharge is far from local thermodynamic equilibrium (LTE). The existence of LTE implies that all species at a given point in space and time have the same temperature. Indeed, the term "temperature" has no meaning in the absence of LTE. In discharges of interest in plasma processing, charged species (electrons and ions) are in general at elevated energies compared with the energy of neutral species because of the electric field. Usually, ions are near the neutral gas temperature, but electrons have a much higher mean energy, because most collisions between charged and neutral species are elastic (i.e., there is no change in internal energy; only kinetic energy

is exchanged between particles). The fraction of energy exchanged in an elastic collision is a function of the relative masses of colliding particles. For particles of similar mass, kinetic energy is exchanged readily (e.g., one billiard ball can lose all of its momentum to another in a collision). However, a small particle loses only a small fraction of its kinetic energy when colliding with a much heavier particle. The fraction of kinetic energy transferred is proportional to twice the smaller mass divided by the sum of the small and large masses. However, if the relative energy of colliding particles is sufficiently high, then inelastic collisions can occur. These processes have been described in the list on page 384.

Solutions to the Boltzmann Equation for Discharges. In conventional chemically reacting systems, all species are assumed to have the same distribution of energies, namely the well-known Maxwell–Boltzmann distribution. This assumption is incorrect for discharges at low pressure because of the large deviation from LTE. Because the rates of important electron–neutral species inelastic collision processes such as molecular dissociation depend on the form of the electron energy distribution function rather than on mean energy (equation 3), such assumptions can create serious problems in the modeling of discharges. The calculation of the distribution function for electrons and ions is not a simple task, particularly under the extreme conditions of a discharge. The normal procedure for obtaining the electron velocity distribution function in a weakly ionized gas is to solve the Boltzmann equation (15, 54–56):

$$\frac{\partial f}{\partial t} + \frac{\mathbf{v} \cdot \partial f}{\partial \mathbf{x}} + \frac{e\mathbf{E}}{m} \cdot \frac{\partial f}{\partial \mathbf{v}} = \left(\frac{\partial f}{\partial t} \right)_{\text{collisions}} \quad (4)$$

where f is the velocity distribution function, t is time, \mathbf{x} is position, \mathbf{v} is velocity, \mathbf{E} is the electric field, e is the charge on the electron, and m is electron mass. Equation 4 gives the rate at which the distribution function changes because of collisions.

The Boltzmann equation works reasonably well when electrons collide mainly with neutral species. Electron–electron or electron–ion collisions involve coulombic interactions that have a longer range than that of electron–neutral species interactions. Coulombic-interaction potentials vary inversely with separation, but electron–neutral species interaction potentials vary inversely with the fifth or sixth power of separation.

Most of the work in solving the Boltzmann equation for electrons has been for the relatively simple conditions of electron swarm experiments. In these experiments, electrons are released from a cathode in low concentrations and drift under the influence of a uniform applied electric field in a low-pressure gas towards an anode at which the electrons are collected. If

the electrons are released as a pulse, then the time for electrons to drift to the anode is a measure of electron mobility. If the radial and axial spreads of the electron pulse can be measured at the anode (with a radially segmented electrode, for example), then a measure of the electron longitudinal and transverse (with respect to the direction of drift) diffusivities can be obtained. Further, if electrons are created through ionization or lost through electron attachment, then rate coefficients for these processes can be determined. Such experiments provide rate and transport coefficients but not collision cross sections.

To deduce cross sections, the following iterative process is used. A trial set of cross sections is chosen, the Boltzmann equation is solved numerically, and the corresponding rate and transport coefficients are calculated. If the measured and predicted coefficients fail to agree, a revised set of cross sections is chosen, and the process is repeated until satisfactory agreement is reached.

A great deal of research has gone into improving the procedures for solving the Boltzmann equation (57) in the context of electron swarm experiments. Rather than attempt to review this large area, suffice it to say that a considerable amount of work will be necessary to adapt these approaches to conditions in actual discharges. For example, spatial variations, which are neglected or minimized in swarm analyses, are of considerable importance in discharges. In addition, solving for ion characteristics will generally require approaches that are different from those taken for electrons, because ion velocity distribution functions are characterized by large anisotropies in velocity space. Net ion velocity tends to be the same order of magnitude as random ion velocity, a fact that has implications for the techniques used to solve the Boltzmann equation. The most common approach for ions is to solve for velocity moments directly rather than for the distribution function.

An alternative to solving the Boltzmann equation directly is the use of particle simulation techniques, sometimes referred to as Monte Carlo methods (58, 59). Major difficulties with the Monte Carlo approach include self-consistency, inclusion of ions, and extension to two spatial dimensions. However, these difficulties are probably not insurmountable, and the Monte Carlo approach may well turn out to be a very powerful tool for discharge analysis.

Fluid Model of Discharges. An important question is whether it makes sense to attempt to solve for distribution functions or moments in the absence of a commensurate accuracy in the treatment of neutral-species chemistry. As already stated, modeling of the chemically reacting plasma requires solutions to the bulk gas momentum and energy balance equations and continuity equations for each reacting neutral species. Surface chemistry is

incorporated through boundary conditions on species continuity equations, which is analogous to the approach used for thermal CVD (60, 61).

As an alternative to the massive computational effort in coupling Boltzmann or moment equations for each charged species to CVD equations, it may make sense to assume a velocity distribution function for charged species and deal with mean energies. This technique is sometimes referred to as a "fluid" approach, because charged species are treated as if they formed a continuous fluid. In this approach, charged species are treated in nearly the same way as neutral species, except that momentum and energy balance equations are solved for each species. Strictly speaking, this treatment is not correct, because a mean energy does not uniquely determine the value of a rate or transport coefficient. However, this approach is a useful approximation. The major advantage of this approach is that it is much less expensive computationally than solving the Boltzmann equation for each charged species in two velocity dimensions, one or two spatial dimensions, and time. Probably the major disadvantage of the fluid approach is that charged particles may not always behave like a continuous fluid, for example, in high-field sheath regions or where electrons and ions act more like directed beams rather than fluids.

Another point in favor of the simpler, but less accurate, fluid approach is that discharge diagnostics are still quite primitive. In studies of electron and ion swarms, experimentalists routinely measure mobilities and diffusivities with a precision in the order of a few percent. A sophisticated model must be used to properly interpret such experiments. However, for discharges, even relative concentration profiles for a few of the dozens of important neutral and charged species are difficult to attain. Thus, an overly complex and expensive model is probably inappropriate, and the fluid model is a good compromise at present.

Validation of Models. An important goal in establishing the validity of large-scale models of reacting plasmas is to demonstrate agreement between predicted and experimentally measured quantities. This effort has barely begun for plasma processing. Ideally, all fundamental quantities predicted in equations describing discharge physics and chemistry must be measured. Electron and ion densities, net velocity and energy profiles, and the electric field strength profile are all predicted by the discharge physics model, and measurement of these quantities as a function of position and time is helpful. For discharge chemistry models, important variables include neutral-species densities, fluid velocity and temperature profiles, and rates of reaction at surfaces. Many of these quantities are difficult to measure, particularly under realistic etch or deposition conditions.

Some of the most powerful tools for *in situ* discharge diagnostics are optical (62). Plasma-induced emission spectroscopy, laser-induced fluorescence, laser absorption, and laser optogalvanic spectroscopy have all been

recently applied in discharge diagnostics. Considerable work remains in the development of these tools so that systematic and comprehensive measurements can be compared with model predictions.

Plasma Processes versus Combustion. To model discharge chemistry, detailed mechanisms and rate coefficients for all elementary reactions are required. This requirement represents a large amount of information even for simple systems. By analogy, for the combustion of hydrogen, a typical model would include eight species (H_2 , O_2 , H_2O , O , OH , H , HO_2 , and H_2O_2) and about 20 elementary reactions. This case is probably the simplest nontrivial combustion problem. Computationally, the major expense is in the number of species, because a continuity equation for each species must be solved. As the complexity of the set of reactants increases, the number of intermediate reactants and elementary reactions increases, and the computational costs rise correspondingly. The inclusion of all important species is not always clear, and values for rate coefficient parameters can be difficult to obtain. In particular, the measurement of reaction rates is not easy when intermediate radical species are involved. Intermediate species are not stable and will sooner or later react to form other species. Sampling of these species is difficult, and estimates of rate coefficients can vary widely.

Combustion modeling is a good paradigm for plasma process modeling because the goals and problems involved are similar. For both, interest is in predicting the detailed chemistry of many different reactive species. Both gas-phase and surface reactions are important, and physical processes must be included in models. For combustion, chemistry interacts strongly with fluid mechanics and heat transfer. One area of combustion research that the plasma analyst, thankfully, can ignore is the study of turbulent reacting flows. At the low pressures encountered in plasma systems, flows are virtually always laminar. The plasma modeler has many other unique difficulties, however, including the possibility that at sufficiently low pressures (i.e., <6.7 Pa), the system may no longer be treated as a continuum, because mean free paths can be in the same order as reactor dimensions.

A perspective on the status and prospects of detailed plasma modeling may be gained by examining the present situation in combustion modeling (63). Currently, the only fuels that can be modeled with real confidence are pure hydrocarbons (no nitrogen or sulfur) that have at most two carbon atoms. When particulates form during combustion or when combustion occurs at solid surfaces, confidence in the model drops substantially. The presence of trace species such as nitrogen and sulfur complicates matters further. This state of relative ignorance in combustion is particularly striking because combustion chemistry has been studied fairly intensely for decades. In contrast, the present status of plasma chemistry research indicates that only the first stumbling steps have been taken; a great deal of work is yet to be done. The plasma-process-modeling community can, however, take

advantage of progress made in related areas such as combustion and CVD by initially adopting approaches and techniques that have proved successful.

System of Model Equations. Because of the tremendous complexity of the processes involved in plasma chemical reactors, the number of possible sets of model equations is large. In the following treatment, one set of equations is presented, but this set is by no means exhaustive.

Qualitatively, to model the chemically reacting plasma, neutral-species chemistry and transport and the electrical or plasma physics aspects of the discharge must be considered. The chemical and physical properties included in the model of the discharge must at least reflect the current understanding of the most important processes. The conventional view of discharge behavior has been described previously, but will now be reviewed briefly to set the stage for equation formulation.

Current Understanding of Discharge Behavior. Electron-impact dissociation of neutral reactant molecules creates highly chemically reactive radicals that can react further in the gas phase and diffuse and convect to surfaces where they react to form or etch films. The surface chemistry is substantially influenced by the action of ions bombarding the surface. To model the chemistry of neutral reactants, a continuity equation for each chemically important species must be solved. These continuity equations must include important transport terms (convection of bulk gas and diffusion) and creation-and-loss terms (electron-impact creation or loss and neutral species–neutral species gas-phase reactions). To account for bulk gas convection, equations for bulk gas momentum and overall mass continuity must be solved. In addition, because surfaces in plasma deposition reactors are often heated to temperatures of 300 °C or higher and because both gas-phase chemistry and gas density depend on temperature, an energy balance for gas temperature must be solved. In plasma etching systems, surfaces may not be heated, and so the energy balance may not be required. This set of equations—continuity for each species, momentum, mass, and energy—are generally required for any reacting flow.

Often, to simplify the analysis, the gas is assumed to be well mixed or to flow as a plug with no diffusion. In the well-mixed system, no gradients exist, and the set of coupled partial differential equations becomes sets of coupled algebraic equations, which is an enormous simplification. In general, however, spatial variations must be considered.

Formulation of Equations. Discharge structure influences chemistry primarily through electron-impact dissociation and surface ion bombardment. To predict the rate of electron-impact dissociation, local electron number density and energy must be known. These quantities are obtained from equations for electron continuity and electron energy, respectively.

Ion bombardment rate is determined from ion momentum or continuity equations, depending upon assumptions made in the model. To solve equations for ion and electron momentum and energy balances, the electric field profile must be known. This profile is obtained from the governing Maxwell equation, which is usually Poisson's equation.

Discharges of interest in plasma processing are usually sustained through the application of radio frequency power to an electrode in the reactor. In this case, a grounded counter electrode is present in the discharge or the entire chamber wall serves as the grounded electrode. Voltages and currents at the powered electrode vary with time, and therefore, quantities in the discharge such as electron density and energy also vary with time. Thus, equations for discharge structure must, in general, include terms for the rate of change of quantities with time, in addition to terms for spatial variations. However, because neutral species respond on a time scale that is much longer than the time scale for charged species, equations describing neutral species do not usually require time derivatives.

Equations for Neutral Species. The balanced equations for neutral species can be expressed in the following form:

$$\nabla \cdot (\mathbf{v} n_s + \mathbf{J}_s) = \sum r_j^s \quad (5)$$

where v is the gas velocity, n_s is the mass density of species s , \mathbf{J}_s is the diffusion flux of species s , and r_j^s is the net rate of creation of species s in reaction j . A sum is made over all such reactions. Gas velocity is obtained from the momentum balance (see equation 7), and reaction rates r_j^s are in general functions of the concentrations of other species and gas temperature, which are obtained from the energy balance (see equation 8). Coupling to gas discharge equations occurs primarily in equation 5 through the role of electron-impact reaction-and-loss terms. In addition, boundary conditions for species continuity equations will include terms for ion-bombardment-enhanced chemical reactions. The equation for total mass continuity is

$$\nabla \cdot (\rho \mathbf{v}) = 0 \quad (6)$$

where ρ is the total gas mass density. The gas momentum balance equation can be expressed as

$$\nabla \cdot (\rho \mathbf{v} \mathbf{v}) = -\nabla p - \nabla \cdot \boldsymbol{\tau} + \rho \mathbf{g} \quad (7)$$

where p is gas pressure, $\boldsymbol{\tau}$ is the viscous stress tensor, and \mathbf{g} is the gravitational force. One form of the energy balance is presented in equation 8

$$\nabla \cdot [(\rho U + p)\mathbf{v} - K\nabla T] = 0 \quad (8)$$

where U is the internal energy of the gas, K is thermal conductivity, and T is temperature. Equation 8 implicitly assumes that gas-phase reactions do not contribute significantly to the energy balance either because rates of reactions are too low or because the enthalpy of reaction is too low.

The equation of state for the gas is given by equation 9, which relates mass density, pressure, molecular weight, and temperature. The molecular weight, M , is assumed to be a mean quantity, because its value depends upon the exact composition of the gas.

$$\rho = pM/kT \quad (9)$$

To be complete, equations 5–9 require boundary conditions. The basis for choosing appropriate boundary conditions is difficult to generalize, partly because the choice of boundary conditions is what differentiates one system from another.

Typically, there are two types of boundaries in reacting flows. The first is a solid surface at which a reaction may be occurring, where the flow velocity is usually set to zero (the no-slip condition) and where either a temperature or a heat flux is specified or a balance between heat generated and lost is made. The second type of boundary is an inflow or outflow boundary. Generally, either the species concentration is specified or the Dankwerts boundary condition is used wherein a flux balance is made across the inflow boundary (64). The gas temperature and gas velocity profile are usually specified at an inflow boundary. At outflow boundaries, choices often become more difficult. If the outflow boundary is far away from the reaction zone, the species concentration gradient and temperature gradient in the direction of flow are often assumed to be zero. In addition, the outflow boundary condition on the momentum balance is usually that normal or shear stresses are also zero (64).

Equation for Electric Field Strength. To include electron-impact source terms in continuity equations for neutral species and to include the effect of ion bombardment on the rate of surface reactions, equations that predict electron and ion densities, momentums, and energy profiles are required. The profiles require an equation for the electric field strength. In general equations for electron and ion continuities (these equations yield electron density and ion density, respectively), electron and ion momentums (for electron and ion net or directed velocity), and electron and ion energies (for electron and ion random or thermal energy) must be solved. Finally, the electric field profile is obtained from Poisson's equation.

This set of equations can be simplified somewhat, depending on discharge operating conditions and on the nature of the discharge gas. For example, in the following equations, electron and ion motions are assumed to be collisionally dominated so electron and ion momentum balance equa-

tions can be simplified. In addition, the positive ions are assumed to exchange energy rapidly in elastic collisions and are therefore at the bulk, neutral gas temperature. This assumption eliminates the need for an ion energy balance. The following equations neglect negative ions, and the gas considered is assumed to be electropositive. This restriction can be easily generalized to include negative ions by incorporating equations for negative ion continuity and momentum.

Electron Continuity Equation. The electron continuity equation is

$$\partial n_e / \partial t + \nabla \cdot j_e = \sum r_j \quad (10)$$

where n_e is the electron density and j_e is the electron flux (see equation 14). The right side represents the sum of all processes that create electrons through ionization, primarily electron-impact ionization of ground-state molecules. For electron-impact processes, the rate is linearly dependent on electron density and the neutral collision partner (equation 2) and usually exponentially dependent on electron temperature. The continuity equation for all other charged species will have a similar form, as shown by the continuity equation for positive ions:

$$\partial n_+ / \partial t + \nabla \cdot j_+ = \sum r_j \quad (11)$$

where n_+ is the positive-ion density and j_+ is the positive-ion flux. The right side represents the sum of all processes that create positive ions through ionization.

In ionization processes, a positive ion is created every time an electron is created, and the net rate of creation of positive ions equals that of electrons. The equation for mean electron energy (referred to as electron temperature) is

$$\partial(3/2n_e k T_e) / \partial t + \nabla \cdot q_e + j_e \cdot e E + \sum H_j r_j = 0 \quad (12)$$

where $3/2 n_e k T_e$ is the mean electron random or thermal energy, q_e is the electron energy flux (see equation 16), j_e is the electron flux, e is the charge on the electron, E is the electric field strength, and H_j is the energy lost in inelastic electron-molecule collisions. The r_j in equation 12 is the rate of all inelastic collisions experienced by electrons. Most of the electron energy is lost via these collisions. Equation 12 is coupled to equations 10 and 11 through the dependence of r_j on mean electron energy.

Electric Field Profile and Electron Energy Flux. The equation that determines the electric field profile through the reactor is Poisson's equation:

$$\nabla \cdot E = e/\epsilon_0(n_+ - n_e) \quad (13)$$

In equation 13, ϵ_0 is the permittivity of free space. Poisson's equation is the governing Maxwell equation, and use of this equation is justified by the fact that the wavelength of the radio frequency field is large compared with discharge dimensions. If this situation were not true (as in the case of microwave discharges), then the complication of electromagnetic wave propagation in the discharge has to be treated. The electron and ion momentum balance equations are simplified by the assumption that charged-particle motion is dominated by collisions. In this case, momentum balance equations for electrons and ions reduce to the following:

$$\mathbf{j}_e = -D_e \nabla n_e - \mu_e n_e \mathbf{E} \quad (14)$$

$$\mathbf{j}_+ = -D_+ \nabla n_+ + \mu_+ n_+ \mathbf{E} \quad (15)$$

Both equations 14 and 15 contain a diffusion term, D , for diffusivity and a drift term, μ , for mobility. For positive ions, the diffusion term is nearly always negligible compared with the drift term, but both terms are retained for reasons that have to do with numerical stability.

Finally, the expression for electron energy flux is given by

$$\mathbf{q}_e = -(5/2)n_e D_e \nabla T_e + 5/2n_e k T_e \mathbf{j}_e \quad (16)$$

where the first term on the right side of the equation accounts for electron random motion (thermal conduction) and the second term accounts for energy transported by electron-directed motion.

Boundary Conditions. To complete the set of equations for the discharge physical structure, boundary conditions are needed. One possible set of boundary conditions is presented in Table II.

Boundary conditions for electron density, ion density, and electron energy are all "flux" boundary conditions, wherein an expression is given for the flux of the quantity over which the balance is made. The net flux of electrons to the surface (assumed to be conducting) is the difference between the rate of recombination and the rate of creation through secondary electron

Table II. Boundary Conditions for Fluid Equations

Boundary Condition	Physical Significance
$\mathbf{n} \cdot \mathbf{j}_e = n_e (kT_e/2\pi m_e)^{1/2} - \gamma \mathbf{n} \cdot \mathbf{j}_+$	Electron flux balance ^a
$\mathbf{n} \cdot \mathbf{j}_+ = \mu_+ n_+ \mathbf{E} \cdot \mathbf{n}$	Ion flux balance
$V = V_{dc} + V_{rf} \sin(2\pi\nu t)$	Voltage boundary value
$\mathbf{n} \cdot \mathbf{q}_e = n_e (kT_e/2\pi m_e)^{1/2} (3/2kT_e) - \gamma \mathbf{n} \cdot \mathbf{j}_+ (3/2kT_{ec})$	Electron energy flux balance
$F(x, t) = F(x, t_p)$	Periodicity conditions on all solutions

^aThe electron flux balance is equal to rate of recombination – rate of emission.

emission. The boundary condition for positive ions is that the flux is due only to drift motion. The flux of electron energy is assumed to result from a balance between energy lost through recombination and energy gained through secondary emission. This boundary condition is subject to criticism, because effects due to the work function for the surface and energy of impinging ions have been neglected. However, preliminary solutions show that the important features of the electron energy profile are not strongly affected by the simplified form of the boundary condition.

The boundary condition for Poisson's equation is to specify voltage at the conducting surfaces. Some workers have suggested that a more stable numerical solution results from a specification of current at the boundary rather than voltage. Typically, one electrode is grounded and the other is powered. In the model, the grounded electrode is assigned zero voltage, and the powered electrode can have a dc bias voltage (as discussed earlier), in addition to the rf voltage. In fact, the actual voltage wave form at the powered electrode is a consequence of the external circuit, including the power supply, matching network, and cables. Simple specification of the voltage at the powered electrode is an approximation, but in many cases, this approximation can be done with acceptable error. An obvious extension would be to solve an equation representing the external circuit at the electrode for the voltage.

The solutions sought in the discharge simulation are time periodic and match the normal stable operating conditions in the discharge. Time periodicity in the solutions is driven by the time-varying voltage at the powered electrode. The time periodicity condition is expressed as

$$u(x, t) = u(x, t + t_p) \quad (17)$$

where u is any function in the simulation, x is position in the discharge, t is time, and t_p is the rf period ($t_p = 1/v$, where v is frequency in hertz).

The numerical solution of the discharge equations and boundary conditions can be approached by using either finite-difference or finite-element methods to make the spatial derivatives discrete. The resulting set of coupled, nonlinear ordinary differential equations can be solved by using relatively standard methods. Typically, the equations are integrated with respect to time until the desired time-periodic solution is obtained. In fact, obtaining a numerical solution is by far the most difficult part of the entire modeling exercise. The set of coupled, nonlinear partial differential equations is stiff, with widely varying temporal and spatial scales in the solution. The size and nonlinearity of the set of coupled equations require either a dedicated minicomputer or a supercomputer for reasonable solution times. Preliminary solutions have been obtained (65) but a great deal of work remains before this modeling approach becomes well established.

Other Modeling Approaches. The modeling just outlined should be viewed in the context of previous models of plasma chemical reactors. A representative list of models of plasma chemical reactors is presented in Table III (66–84), with brief descriptions of the following characteristics of each model: reactor type, chemistry studied, transport model for neutral species, and treatment of discharge physics. One of the reasons for the detailed discussion of the discharge fluid equations is that discharge physics seems to be the part of plasma chemical reactor models that is the least well understood and is probably the major source of mystery concerning reactor behavior. Other than the fluid model just described, the only treatment of spatially and temporally dependent discharge behavior involves the use of a (non-self-consistent) Monte Carlo technique (79) to describe electron dynamics.

Most of the models assume that neutral-species transport can be represented with either a well-mixed model or a plug flow model. The major drawback to these assumptions is that important inelastic rate processes such as molecular dissociation are usually localized in space in the reactor and are often fast compared with rates of diffusion or convection. As a result, the spatial variation of fluid flow in the reactor must be accounted for. This variation introduces a major complication in the model, because the solution of the nonisothermal Navier–Stokes equations in multidimensional geometries is expensive and difficult.

The most glaring drawback of most of the models presented heretofore is the lack of proper experimental verification. Model predictions must be compared with experimental measurements in order to verify the model. If the model assumes that concentration gradients are negligible, then this assumption should be tested. If the model predicts detailed spatial- and time-dependent profiles, then these profiles must be measured and compared with the predictions. Only when such comparisons have been made and measurements and predictions agree over a wide range of conditions can the model be considered accurate.

Detailed models of plasma chemical reactors are just beginning to be developed. The combination of neutral-species chemistry, hydrodynamics, and discharge physics is sufficiently complex that modeling lags behind both industrial practice and even certain diagnostics such as laser spectroscopy and molecular-beam mass spectrometry. However, the widespread availability of large-scale computers, coupled with an increasing interest in a fundamental understanding of plasma processes, will spur the continued development of mathematical modeling and numerical solutions of model equations.

Etching of Thin-Film Materials

The basic principle behind etching a solid material with a reactive gas discharge is inherently simple. A gas is chosen that dissociates into reactive

species that can form a volatile product with the material to be etched. However, a viable etch process must also display reasonable etch rates, good selectivity, and directional (anisotropic) etching. All of these criteria can be met by judicious choice of reactant gases and plasma conditions. For instance, because etch rates usually follow an Arrhenius dependence on substrate temperature and because the effective activation energy is material dependent, etch rate and, thus, selectivity vary exponentially with temperature. Also, ion bombardment generally imparts different degrees of damage to various materials; thus, etch selectivity can be altered to tailor a specific etch process by changing the ion bombardment energy.

Most isotropic etchants exhibit a loading effect, wherein a measurable depletion of the active etchant results from consumption in the etch process. In these cases, the overall etch rate depends upon the area of film to be etched. Under extreme circumstances, with carbon-based etch gases, etchant depletion can be so severe that polymer deposition occurs instead of etching. An analysis (85) of the loading effect, which has been extended (86) to include multiple etchant loading and other etchant loss processes, indicates that the etch rate (R) for N wafers each of area A is given by

$$R(N) = \frac{(k_{\text{etch}}/k_{\text{loss}})G}{1 + (k_{\text{etch}}\rho NA/k_{\text{loss}}V)} \quad (18)$$

where k_{etch} and k_{loss} are the rate constants (first order) for etching and etchant loss in an "empty" reactor, respectively; ρ is the number density of substrate molecules per unit wafer area in the reactor; G is the generation rate of the active etchant species; and V is the volume of the reactor. This formalism indicates that as the number of wafers (or wafer area) increases to a point where $k_{\text{etch}}\rho NA/k_{\text{loss}}V \gg 1$, the etch rate

$$R(N) = GV/\rho NA \quad (19)$$

varies inversely with the number of wafers. This dependence is characteristic of a marked loading effect and shows that loading effects can be controlled to some extent by using large-volume reactors. Further, these effects can be eliminated when homogeneous or heterogeneous etchant loss dominates ($k_{\text{loss}} \gg k_{\text{etch}}$). When ion bombardment controls the reaction, equation 18 is inapplicable, because the etch rate is determined by bombardment flux rather than etchant supply.

Other transport limitations, such as diffusion-controlled reactions, can lead to localized depletion of etchant, which results in a number of observable etch effects. The size and density of features can influence the etch rate at different locations on a single wafer and thus produce pattern sensitivity. Depletion across a wafer produces a bull's-eye effect, whereas depletion across a reactor is indicated by the fact that the leading wafer edge etches faster than the trailing edge. Similar effects are noted when product removal

Table III. Discharge Reactor Models

<i>Reactor Type</i>	<i>Chemistry</i>	<i>Transport</i>	<i>Discharge Physics</i>	<i>Reference</i>
Parallel-plate electrodes	Ethane polymerization	Plug flow with axial dispersion	Assumed average electron density and energy	66
Parallel-plate with electric barriers	Helium discharge	Not applicable	Ambipolar diffusion model	67
Flow through plasma then afterglow	CO oxidation; CO ₂ dissociation	Axial plug flow	Mean electron density and energy	68
Parallel-plate pyrex pillbox	Oxygen dissociation	Plug flow	Cosine electron density between parallel-plate electrodes	69
Radio frequency diode reactor	Silane decomposition	Well mixed	Mean electron density and energy	70
Cylindrical tube with ring electrodes	Silane decomposition and dispersion	Plug flow with axial dispersion	Mean electron density measured with interferometry	71
Inductive coupling to quartz tube	Silicon nitride from silane–N ₂	Plug flow	Mean electron density measured with microwave interferometry	72
Tubular and radial	No specific chemistry	Parabolic flow	Dissociation rate coefficient treated as a parameter	73
Arbitrary	No specific chemistry	Well mixed	Not treated	74
Parallel-plate electrodes	C _n F _m in H ₂ and O ₂ to etch Si and SiO ₂	Well mixed	Mean electron density from power balance; electron energy distribution from Boltzmann code	75
Tubular reactor with afterglow	CF ₄ etching Si	Plug flow	Assumed mean density and energy in discharge	76

Flow between parallel-plate electrodes	SF ₆ etching silicon	Plug flow	Boltzmann equation and Monte Carlo for electron energy; electron density power balance	77
Flow between parallel plate electrodes	SF ₆ -O ₂ etching silicon	Well mixed	Boltzmann equation for electron energy; power balance for electron density	78
Parallel-plate electrodes	SiH ₄ dissociation in silane-Ar mixtures	Not treated	Spatially and temporally dependent Monte Carlo treatment for electrons; electric field is assumed	79
Parallel-plate electrodes; downstream plasma	SiH ₄ dissociation for Si films; both thermal and plasma dissociation methods	Two-dimensional nonisothermal Navier-Stokes	Assumed electron density and energy	80
Hollow cathode	NF ₃ etching	Well mixed	Electron density and energy treated as adjustable parameters	81
Parallel-plate reactor	Dissociation of CH ₄ for amorphous carbon	Well mixed	Mean electron density; energy distribution measured with Langmuir probe	82
Barrel etcher with etch tunnel	Arbitrary between wafers	Diffusion	Not applicable	83
Parallel-plate radial flow	CF ₄ etching Si	Two-dimensional isothermal Navier-Stokes	Ambipolar diffusion with assumed electron density and energy	84

is transport limited. Pressure and flow interact by determining the residence time relative to diffusion, convection, and reaction rates. Residence times that are short compared with reaction times will reduce diffusion limitations, whereas long residence times will enhance them.

Most of the effects just discussed can be reduced by the judicious choice of pressure and flow rates. However, good or even adequate process control requires precise termination of the etch sequence by using suitable endpoint detection or plasma-diagnostic schemes. Numerous methods have been invoked to follow plasma processes either by monitoring film thickness *in situ* or by detecting changes in plasma composition or impedance. Discussion of these optical, chemical, electrical, or physical techniques and their application to plasma etching (or deposition) is beyond the scope of this chapter; however, recent publications cover this important area in great detail (2, 62, 87–89). Finally, if process design rather than diagnostics is desired, response surface methodology (statistical design) can be invoked (90, 91). This technique permits the determination of a parametric operating window for a particular complex process with the execution of a minimal number of experiments. Unfortunately, no fundamental insight into the effect of specific variables on the etch process is generated.

Etch Models. As has been discussed, an extensive parameter space is associated with plasma techniques. Therefore, if the development of etch processes is to proceed efficiently, some means of data assimilation and prediction must be available. Two general schemes have been proposed to organize chemical and physical information on plasma etching. Both schemes deal primarily with carbon-containing gases, but with a slight modification, they can be easily applied to other etchants. Conceptually, the two models are similar, although they emphasize different aspects of plasma etching.

F/C Ratio Model. The fluorine-to-carbon ratio (F/C) of the active species can be used (92) to explain the observed etch results (Figure 8). This model does not consider the specific chemistry occurring in a glow discharge but, rather, views the plasma as a ratio of fluorine species to carbon species that can react with a silicon surface. The generation or elimination of the active species by various processes or gas additions then modifies the initial F/C ratio of the inlet gas.

The F/C ratio model accounts for the fact that for carbon-containing gases etching and polymerization occur simultaneously. The process that dominates depends upon etch gas stoichiometry, reactive-gas additions, amount of material to be etched, and electrode potential and upon how these factors affect the F/C ratio. For instance, as described in Figure 8, the F/C ratio of the etchant gas determines whether etching or polymerization is favored. If the primary etchant species for silicon (F atoms) is consumed either by a loading effect or by reaction with hydrogen to form HF, the F/

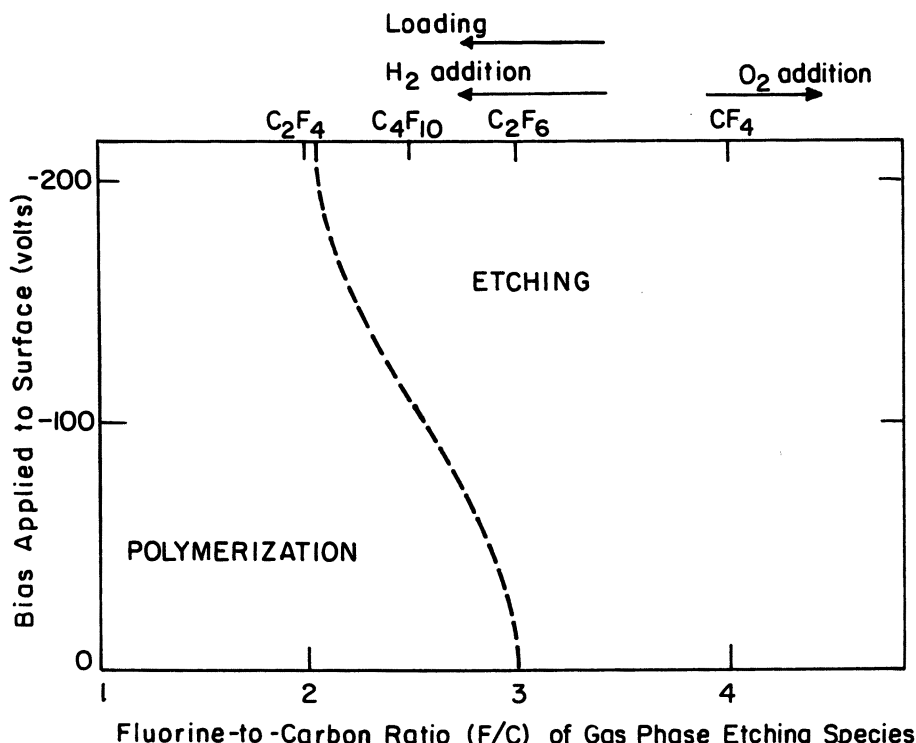
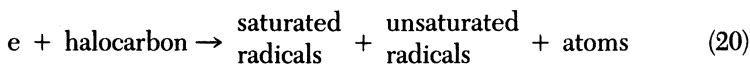
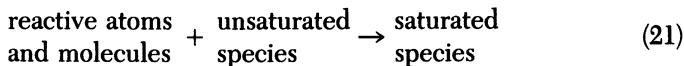


Figure 8. Schematic diagram of the influence of fluorine-to-carbon ratio and electrode bias on etching versus polymerization processes in fluorocarbon plasmas. (Reproduced with permission from reference 92. Copyright 1980 Springer-Verlag New York, Inc.)

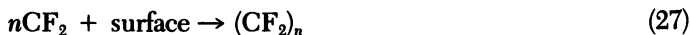
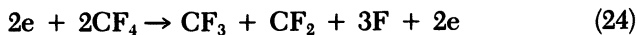
C ratio decreases, thereby enhancing polymerization. However, if oxygen is added to the etchant gas, reaction with carbon-containing fragments to form CO or CO_2 can occur, thus increasing the F/C ratio and favoring etching. Further, as the negative bias of a surface exposed to the plasma increases at a constant F/C ratio, etching of this surface becomes more important relative to polymerization. Such effects are caused primarily by the enhanced energies of the ions striking these surfaces that result in polymer sputtering.

Etchant-Unsaturated Species Model. In the etchant-unsaturated species model described by equations 20–23 (93), specific chemical species derived from electron collisions with etchant gases are considered.





Application of this model to a CF_4 plasma results in the chemical scheme indicated by equations 24–27.



Depending upon the particular precursors generated in the gas phase, etching, recombination, or film formation (i.e., polymerization) can occur. Also, gas-phase oxidant additives (O_2 , F_2 , etc.) can dissociate and react with unsaturated species. Mass spectrometric studies of oxidant additions to fluorocarbon and chlorocarbon gases have demonstrated that the relative reactivity of atoms with unsaturated species in a glow discharge follows the sequence $\text{F} \sim \text{O} > \text{Cl} > \text{Br}$ (93). The most reactive species present will preferentially undergo saturation reactions that reduce polymer formation and that may increase halogen atom concentration. Ultimately, the determination of the relative reactivity of the plasma species allows the prediction of the primary atomic etchants in a plasma of specific composition.

Specific Materials. Because the fundamental physics and chemistry of reactive gas discharges used for etching is not yet fully understood, empirical approaches to the design of etch processes abound. As indicated earlier, etchant selection begins with considerations of product volatility. Virtually any gas or vapor that can dissociate to form etchant species has been considered or studied. An abbreviated list of the most common reactant molecules used to etch films of interest in electronic materials processing is given in Table IV.

Generally, a single etchant species is not used in production processes; rather, mixtures of gases or vapors are used to tailor the etch process to establish a particular rate, selectivity, anisotropy, etc. Often, the additives include inert gases such as Ar or He. These gases are responsible for Penning processes that enhance dissociation and ionization. Further, these gases can stabilize and homogenize discharges that oscillate between multiple states (94). In the following sections, etch considerations for individual materials are discussed.

Table IV. Etch Gases Used for Various IC Film Materials

Film	Gases
Si	CF ₄ , CF ₄ -O ₂ , CF ₃ Cl, CCl ₄ , SF ₆ -O ₂ , SiF ₄ -O ₂ , NF ₃ , ClF ₃
SiO ₂	C ₂ F ₆ , C ₃ F ₈ , CF ₄ -H ₂ , CHF ₃
Si ₃ N ₄	CF ₄ -O ₂ , C ₂ F ₆ , C ₃ F ₈ , CF ₄ -H ₂
Organic materials	O ₂ , O ₂ -CF ₄ , O ₂ -SF ₆
Al	CCl ₄ , CCl ₄ -Cl ₂ , BCl ₃ , BCl ₃ -Cl ₂ , SiCl ₄
W, WSi ₂ , Mo	CF ₄ , C ₂ F ₆ , SF ₆
MoSi ₂	NF ₃
Au	C ₂ Cl ₂ F ₄ , Cl ₂
Cr	Cl ₂ -O ₂ , CCl ₄ -O ₂

NOTE: Often, inert gases such as Ar or He are added to the mixtures.

Silicon and Polysilicon. The isotropic etching of silicon and polycrystalline silicon (poly-Si) by atomic fluorine (F) is probably the most completely understood of all etch processes, particularly for the cases in which F atoms are produced in discharges of F₂ (95) and CF₄-O₂ (96). Fluorine atoms etch <100>-oriented Si at a rate (in angstroms per minute) given by (95)

$$R_F(Si) = 2.91 \times 10^{-12} T^{1/2} n_F \exp(-0.108 \text{ eV}/kT) \quad (28)$$

where n_F is the F atom concentration per cubic centimeter, T is the temperature (in kelvin units), and k is Boltzmann's constant. The combination of these and other studies (97, 98) has generated a reasonably detailed mechanism of silicon etching in F-containing discharges, in which the major etch products are SiF₂ and SiF₄ (2, 99). Fluorine atoms chemisorb onto clean silicon surfaces to form a stable SiF₂-like steady-state surface under low-pressure (0.013 Pa) conditions (98, 100a).

However, during conditions of higher pressure, SiF₃ moieties are the primary species detected on Si surfaces (100b). Continued reaction requires that the fluorinated surface layer be penetrated by impinging F atoms. The reaction probability for this step is low (<0.01) at normal substrate temperatures (95); thus, the penetration is rate limiting and proceeds at a rate defined by equation 28. Further, most F-containing etchant gases display similar apparent activation energies (~0.1 eV per atom) so that the same mechanism and etchant (F atoms) are probably operative in these somewhat different chemical systems.

Gases such as CF₄ and SF₆ offer advantages because of their low toxicity; however, the formation of unsaturated species such as C_xF_{2x} and S_xF_{2x} in the discharge can scavenge free F atoms and, in extreme cases, can lead to significant polymer or residue formation. The role of oxygen in these plasmas is twofold. First, in accord with the etchant-unsaturated species model, O atoms react with unsaturated species to enhance F atom generation and to

eliminate polymerization. Second, with sufficient O₂ present, O₂ or O can occupy film adsorption sites and thus inhibit etching (96, 101). Gases such as NF₃ and ClF₃ (81, 86, 102) are interesting, because they do not contain atoms that form residues. Therefore, high concentrations of F result without the addition of O₂, which can attack resist materials.

Plasmas that produce chlorine and bromine atoms are excellent for Si etching, because they can generate a high degree of anisotropy. The most commonly used gases have been Cl₂, CCl₄, CF₂Cl₂, CF₃Cl, Br₂, and CF₃Br, along with mixtures such as Cl₂-C₂F₆, Cl₂-CCl₄, HCl-CCl₄, and C₂F₆-CF₃Cl (103-106). High etch rates (500-6300 Å/min for undoped and doped poly-Si) and selectivities (Si:SiO₂ ~ 10-50:1) have been attained. The active etchants in these plasmas are likely to be Cl and Br atoms; however, ion bombardment plays a significant role in achieving high etch rates and anisotropy control (107-110). The high degree of anisotropy that is readily achieved indicates that ion bombardment tends to dominate the etch mechanism by enhancing either the reaction with the chemisorbed SiCl₂ (penetration of Cl into the Si surface) or product volatility. These conclusions are also consistent with the fact that only a small loading effect is observed in Cl-based etching (105), whereas F source plasmas (85, 86) exhibit strong loading effects.

Heavily doped (>10¹⁸/cm³) n-type Si and poly-Si etch faster in Cl- and F-containing plasmas than do their boron-doped or undoped counterparts (103a, 105, 111, 112). Because ion bombardment is apparently not required in these cases, isotropic etch profiles (undercutting) in n+ poly-Si etching often occur. Although the exact mechanisms behind these observations are not completely understood, enhanced chemisorption (103b, 111) and space charge effects on reactant diffusion (112) have been proposed.

Silicon Dioxide and Silicon Nitride. Silicon dioxide can also be etched by F atoms in a downstream discharge configuration. However, because of the strength of the Si-O bond, etch rates (equation 29) are low without particle bombardment (95).

$$R_F(SiO_2) = 6.14 \times 10^{-13} n_F T^{1/2} \exp(-0.163 \text{ eV}/kT) \quad (29)$$

XeF₂ does not etch SiO₂ in the absence of bombardment (39). Thus, F and XeF₂ are not equivalent sources of F atoms, probably because of differences in sticking coefficients and the Xe-F bond energy. Because ion-bombardment-assisted etching of SiO₂ occurs in F-containing gases, directional etching can be achieved. This fact suggests that the etchants described for Si are suitable for etching oxide and nitride; however, they can be used only in the absence of silicon. Therefore, selective etching of these materials represents an important application of the chemical models presented earlier.

(*see* Etch Models). The earliest reported etchant gases for selectively etching SiO_2 and Si_3N_4 in the presence of silicon were $\text{CF}_4\text{-H}_2$, CHF_3 , C_3F_8 , and C_2F_6 (113). Selectivities as high as 15:1 ($\text{Si}_3\text{N}_4\text{:Si}$) and 10:1 ($\text{SiO}_2\text{:Si}$) were achieved. However, these selectivities are lower than one would like for a production process. All of these plasmas tend to be fluorine deficient, a fact suggesting that CF , CF_2 , or CF_3 might be active etchants (114). In any case, carbon-containing species are clearly involved in the etch mechanism, because in addition to SiF_4 , products such as CO and COF_x have been observed by mass spectrometry (114–116) during SiO_2 and Si_3N_4 etching.

To achieve selective oxide and nitride etching, additives to F source plasmas are chosen to make a F-deficient chemical environment. Additives include H_2 , C_2H_4 , and CH_4 , which are efficient F scavengers. Alternatively, molecules that contain F, C, and H are used, such as CHF_3 . Deciding the amount of additive necessary remains more of an art than a science, because oxide and nitride selectivity requires operation in a chemical environment very close to the demarcation between etching and polymerization shown in Figure 8. In fact, polymer deposition on Si generally occurs while active etching of oxide proceeds (103c, 117, 118). Thus, the mechanism for selective oxide and nitride etching may not involve CF_x as primary etchants but as film formers that inhibit Si etching by passivating chemisorptive sites.

An example of the improvement in selectivity with $\text{CF}_4\text{-H}_2$ mixtures is shown in Figure 9 (118). With no added H_2 , the selectivity of silicon dioxide over silicon ($\text{SiO}_2\text{:Si} \sim 1.3$) is unacceptable for a controllable process. However, as H_2 is added, F atoms are scavenged (to form HF), and thus the C/F ratio of unsaturated species in the gas phase is increased (Figure 8 or equations 24–27), and polymerization is promoted. Because oxygen is released from SiO_2 as it etches, carbonaceous residues can be removed (as CO , CO_2 , or COF_2) from this material. On Si, no mechanism other than sputtering is available for carbon removal; thus, the carbon deposits inhibit etching even with low H_2 additions. The small decrease in SiO_2 etch rate with increasing H_2 is probably a result of etchant dilution. At 40% H_2 , a selectivity of ~40 ($\text{SiO}_2\text{:Si}$) is achieved under the designated conditions of pressure, power, etc. (118). If more H_2 is added, polymerization on SiO_2 surfaces retards etching still further.

The qualitative role of ions in promoting oxide and nitride selectivity has also been established. Discharge conditions (i.e., pressure and voltages) are generally those that favor ion-enhanced reactivity, and ion bombardment is usually required to initiate etching (117). The absence of a noticeable dependence on substrate temperature (119), minimal loading effects (120), and the sensitivity of etch rate with respect to electrode (121) and sheath potential (104) reinforces the importance of ion bombardment. In one study (121), selective etching of SiO_2 over Si by >50:1 was obtained in a CHF_3 plasma by using cathode (powered-electrode) coupling, whereas selectivities of <10:1 were observed at the anode.

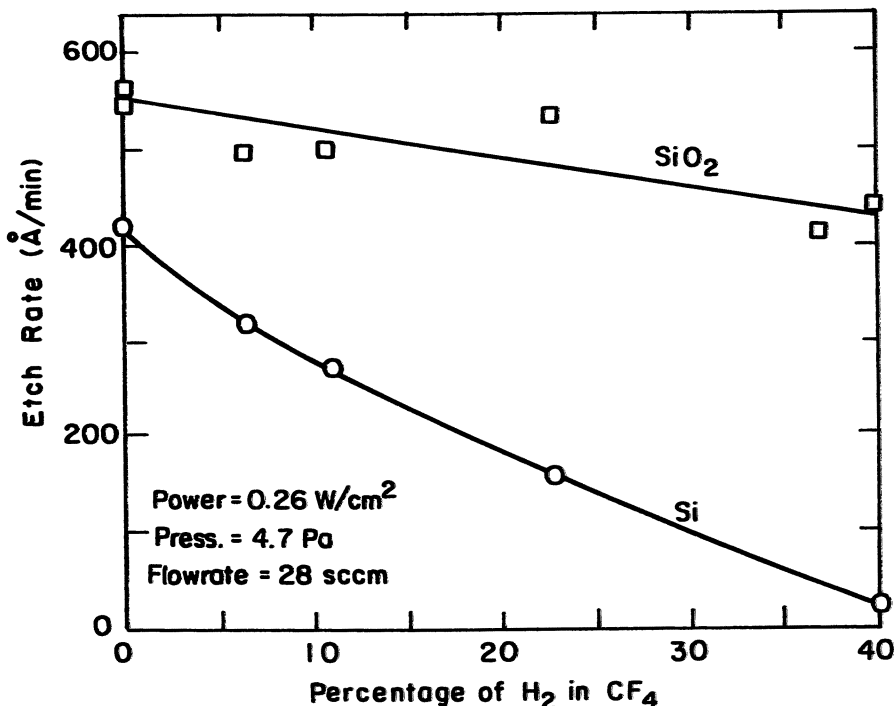


Figure 9. Dependence of silicon and silicon dioxide etch rates on the percentage of H₂ in CF₄-H₂ plasmas. (sccm is standard cubic centimeters per minute.) (Reproduced with permission from reference 118. Copyright 1979 The Electrochemical Society, Inc.)

Group III-V Materials. Group III-V semiconductor compounds such as GaAs, GaP, InP and GaAlAs form the basis for many new electronic applications, particularly high-speed integrated circuits (ICs) and microwave and optoelectronic devices. The development of plasma pattern delineation methods is an area of active research because of the parallelism with the more highly developed silicon technology; however, these systems are somewhat more complicated. Because most of the applications involve binary, ternary, and even quaternary alloys, suitable etchants must be capable of selective etching when stoichiometric changes are made to obtain specific device characteristics.

At present, primarily the binary compounds have been studied, and considerations of product volatility are the most significant driving force behind much of this research. The group III-V compounds are particularly difficult, because the group V elements form volatile halides, whereas group III halides, particularly the fluorides, tend to be involatile. As a result, F source plasmas, which have been the mainstay of silicon technology, are

generally not practical for the etching of group III-V materials unless high ion bombardment energies are used. H₂ discharges have been used to etch group III-V materials (122). Temperatures above 100 °C were used, selectivities of GaAs oxide to GaAs were low (~2), and etch rates of the oxide were reasonable (<20 Å/s). However, GaAs etching displayed undercut profiles.

Because of the problems just described, most studies have used chlorine-containing plasmas with elevated substrate temperatures to take advantage of the volatility (albeit limited) of the group III chlorides. The importance of the volatility concept in the etching of group III-V materials relative to the reaction concepts that dominate Si etching is evident from results of chlorine-rich vapors. When gases such as CCl_xF_{4-x} (where x = 2, 3, or 4), COCl₂, PCl₃, BCl₃, SiCl₄, HCl or Cl₂ are used in rf (usually RIE configurations) or dc plasmas, the etch rates of GaAs and other group III-V compounds increase substantially (123–130).

Br₂ discharges have also been used to etch GaAs (127). These studies were performed under conditions in which isotropic etch profiles or chemical etching occurred. Because the chemical compositions (Ga/As ratio) of the different atomic planes in GaAs vary, crystallographic etch patterns are observed under etch conditions in which chemical processes dominate. Similar results are noted for Cl₂ plasmas. Furthermore, pure Br₂ vapor (no plasma and, thus, no Br atoms or particle or photon bombardment) etches GaAs, and smooth surfaces are observed (127). By using absorption spectroscopy to determine absolute Br concentrations in discharges, the etch rate of GaAs is found to be proportional to the Br atom concentration (127). In addition, the etch rate increases with frequency (from 0.1 to 14 MHz), in agreement with an increase in Br. Such results are consistent with plasma-etching studies with Cl₂ at 40 Pa, in which the etch rate decreases with decreasing frequency (131).

Temperature plays an important role in the etching of GaAs and InP. Both materials display an Arrhenius dependence on substrate temperature between 200 and 300 °C in Cl₂ discharges (132). The apparent activation energies (34.5 and 10.5 kcal/mol for InP and GaAs, respectively at 40 Pa) are in reasonable agreement with the heats of vaporization of InCl₃ and GaCl₃. Estimates of InP etch rates from kinetic molecular theory, assuming that volatilization of the product (InCl₃) is rate limiting, are in good agreement with the observed rates. However, similar estimates for GaAs are higher than the observed etch rate (132). The investigators conclude that a chemical reaction on the surface must be rate limiting in the case of GaAs, perhaps because of dimerization to form Ga₂Cl₆, which desorbs, or a slow chemical reaction between etchant (presumably Cl) and GaAs (132). Indeed, surface reactions with chlorine have been postulated recently to be rate controlling during the etching of GaAs with a modulated Ar⁺ beam in the presence of Cl₂ molecules (133).

Metals. Because of the high reactivity of most metals with oxygen and water vapor, plasma etching of metals may require more attention to reactor design and process details than is necessary with other materials. Unless the metal forms a volatile oxyhalide or an unstable oxide, water vapor and oxygen must be excluded from or scavenged in the plasma reactor. In addition, the metal–oxygen bond may be extremely strong and therefore ion bombardment is required to assist native-oxide removal.

As a result of ion bombardment effects and of their ability to reduce native oxides chemically, chlorocarbon or fluorocarbon gases, rather than pure halogens, are used typically to etch metal films. However, halocarbon vapors are particularly susceptible to polymerization, which causes residue formation that can interface with etch processes (134).

Aluminum. Aluminum is widely used as an interconnect layer for integrated circuits, and its plasma etch characteristics have been extensively studied (134, 135). Because AlF_3 is not volatile under normal (nonsputtering) plasma etch conditions, chlorine-containing gases (CCl_4 , BCl_3 , SiCl_4 , and CHCl_3) have been the preferred etchants for aluminum (136–139). A few studies have also investigated the use of brominated gases (HBr , Br_2 , and BBr_3) and, consistent with volatility considerations, find results similar to those of chlorinated vapors (140, 141).

An initiation period or a lag time exists at the start of aluminum etching because of scavenging or removal of oxygen and water vapor present in the reactor and etching of the thin ($\sim 30 \text{ \AA}$) native aluminum oxide layer always present on the aluminum surface (136). The removal of oxygen and water vapor can be minimized by using a load lock so that the chamber is not exposed to air or water vapor between etch runs (137) or by using an etch gas (BCl_3 or SiCl_4) that effectively scavenges water and oxygen. Native aluminum oxide can be etched by enhancing the ion bombardment of the surface and by supplying chemical species capable of reacting directly with the oxide, such as CCl_x , BCl_x , or SiCl_x .

After the removal of the native aluminum oxide layer, molecular chlorine (Cl_2) can etch pure, clean aluminum without a plasma (142–144). Indeed, Cl_2 rather than Cl appears to be the primary etchant species for aluminum in a glow discharge (145). At least at low temperature ($<200^\circ\text{C}$), the main product of the etch reaction seems to be Al_2Cl_6 rather than AlCl_3 (146).

To prevent aluminum from spiking through shallow junctions, 1–2% silicon is often added to the film. Because SiCl_4 is volatile at room temperature, aluminum–silicon films can be etched in chlorine-containing discharges.

Copper additions to aluminum films enhance electromigration resistance. However, copper does not form volatile chlorides or other halides, and therefore its removal during aluminum plasma etching is difficult. Two methods can be used to promote copper chloride desorption: increase the

substrate temperature (consistent with the resist material being used) or enhance the ion bombardment so that significant sputtering or surface heating is attained.

After plasma etching is completed, aluminum films often corrode upon exposure to atmospheric conditions. The corrosion is a result of the hydrolysis of chlorine-containing residues (mostly AlCl_3) remaining on the film side walls, on the substrate, or in the photoresist. Because the passivating native oxide film normally present on the aluminum surface is removed during etching, chlorine species are left in contact with aluminum and ultimately cause corrosion. Further, contamination with carbon and radiation damage caused by particle bombardment may enhance corrosion susceptibility (147).

When copper is present in aluminum films, accelerated postetch corrosion is observed. This phenomenon occurs for at least two reasons. Because of the low vapor pressure, hygroscopic CuCl_2 is probably left in contact with the aluminum film, and because most of the copper is present in the grain boundaries as CuAl_2 , the grain boundaries have a cathodic potential relative to the aluminum grains (147). Electrolytic corrosion then takes place upon adsorption of water vapor, followed by hydrolysis of AlCl_3 and CuCl_3 to generate HCl and chlorine ions.

Significant efforts have been made to eliminate or at least minimize corrosion. A water rinse or an oxygen plasma treatment after etching reduces the amount of chlorine left on the etched surfaces, but this step is usually not adequate to preclude corrosion. Low-temperature thermal oxidation in dry oxygen appears effective in restoring a passivating native aluminum oxide film (147). Another method of preventing postetch corrosion is to expose the aluminum film to fluorocarbon plasmas such as CF_4 or CHF_3 (37, 148). This treatment converts the chloride residues into nonhygroscopic fluorides and deposits a fluorocarbon polymer film onto the Al surface so that the Al film can be exposed to ambient conditions without immediate corrosion. Subsequently, a nitric acid rinse can be used to remove the fluoride layer and to regrow the protective oxide.

Chlorine-based plasma etching of aluminum films causes serious degradation of photoresist materials. To some extent, these effects are a result of the etch product, Al_2Cl_6 or AlCl_3 . Aluminum trichloride is a Lewis acid used extensively as a Friedel-Crafts catalyst. Therefore, this material reacts with and severely degrades photoresists (149).

Other Metals. Numerous other metal films have been etched in glow discharges. The following is a brief summary that gives specific information on the etching of the metal films commonly used in VLSI.

After aluminum, the refractory metals and their silicides have been the subject of the most extensive efforts in metal etching (150–155). Because the fluorides and chlorides of the transition metals and silicon are volatile in the presence of ion bombardment, etch studies have been performed with nearly

any fluorine- or chlorine-containing gas. Mixtures of these gases (e.g., SF₆-Cl₂) have also been used. When C or S is present in the reactant gas, oxygen is often necessary to prevent polymer and residue formation and to increase the concentration of fluorine atoms. Oxygen can be added to enhance the transition-metal etch rate, because some oxyfluorides (e.g., those of Mo and W) have reasonable vapor pressures. Layered films (silicide-poly-Si; termed *polycides*) are frequently used to meet specific device requirements. These structures present problems in profile control, and selectivity to underlying SiO₂ or Si materials can be difficult to achieve.

Gold can be etched effectively with C₂Cl₂F₄ (156, 157) or with CClF₃ (158), whereas CF₄-O₂ etching causes staining. The observed staining is believed to be caused by gold oxides, whose formation is enhanced by the presence of atomic fluorine (158). Chromium is etched readily in plasmas containing chlorine and oxygen (159) because of the high volatility of the oxychloride (CrO₂Cl₂). Indeed, the high boiling point of CrCl₂ (1300 °C) results in significantly reduced etch rates of chromium in chlorine plasmas without oxygen.

Titanium can be etched in fluorine-, chlorine-, or bromine-containing gases, because all the titanium halides are volatile. Chlorides and bromides have been studied to a great extent, because they result in high selectivity over silicon-containing films and do not promote staining on gold (158, 160).

Organic Films. Organic films are present during the plasma processing of all materials discussed in the preceding sections, because polymeric resist masks are the primary method of pattern transfer. An ideal mask should be highly resistant to the reactive species, ion bombardment, and the UV radiation produced in the glow discharge and should be readily removed after pattern delineation is complete. However, very high selectivities of the etching film to resist material are not often achieved. As a result, line width loss in pattern delineation frequently occurs as the thinner mask edges erode during etching.

Although CF₄-O₂ plasmas often severely degrade resist materials, resist durability in some plasmas is quite high. For example, conditions favorable for the selective etching of SiO₂ and Si₃N₄ are not as conducive to resist degradation as are CF₄-O₂ plasmas. Thus, CF₄-C₂H₄ (161), CF₄-H₂ (118), CHF₃ (48, 161-163), and C₂F₆-C₂H₄ (119) plasmas exhibit excellent selectivity of oxide over resist even when ion bombardment is present. In these cases, selective oxide etching occurs in a saturated-species-rich plasma near the borderline of polymer deposition, and any degradation of polymeric resist material is likely to be compensated by condensation reactions of saturated species at these sites.

Increased durability can be designed into polymer resists. For instance, for the relative etch rates of a variety of polymers in an O₂ plasma, a high correlation exists between the structural properties of the polymer and their

stability when exposed to the plasma (164). More importantly, the results indicate a synergistic degradation involving atomic oxygen from the plasma and halogen present in either the polymer or the plasma. These studies explain why $\text{CF}_4\text{--O}_2$ discharges produce high mask erosion rates. Atomic fluorine (or chlorine) abstracts hydrogen from the polymer and produces sites that react more readily with molecular oxygen. The etch rate of organic materials in oxygen discharges can be significantly enhanced by the addition of fluorine-containing gases (165, 166). Conversely, oxygen-free plasmas generally result in polymer stabilization. Halogen abstraction of polymer hydrogens followed by reaction with halogen or halocarbon radicals leads to halocarbon groups in the polymer that can make the mask more resistant to plasma degradation.

During the patterning of thin-film materials, two inconsistent demands are imposed on resists. Initially, resists must be highly sensitive to radiation so that exposure times are short. However, after development, the remaining resist should be stable to radiation (plasma) environments. Ion, electron, or photon bombardment from the plasma atmosphere causes heating, sputtering, and the degradation of resists. Thus, efforts to improve temperature control (wafer cooling) and minimize ion bombardment energy have been mounted. Because these approaches are sometimes not effective or are incompatible with profile considerations, methods to toughen resists (particularly AZ [phenol-formaldehyde-based resin] materials) against plasma exposure have been developed.

UV exposure (at $\lambda < 300 \text{ nm}$) of the AZ resist prior to plasma etching causes polymer cross-linking (167, 168) or decomposition (169) of the resist photosensitizer near the surface. Thus, a hardened shell or case is formed that permits a higher bake temperature without resist flow and also reduces the etch rate due to plasma exposure. Exposure to inert plasma (e.g., N_2) causes similar effects (170), possibly because of ion and electron, as well as UV, bombardment of the resist surface. When F-containing discharges are used, fluorination of the resist surface occurs that strengthens the resist (because of the formation of C–F bonds) and minimizes reactivity (171).

Oxygen plasmas provide a highly selective medium for the removal of organic materials and have been used extensively for stripping photoresists (172–176), removing epoxy smears from other electronic components, and etching printed circuit boards (177). In addition, the use of oxygen plasmas in delineating the original mask pattern is of interest. Termed “plasma-developable resists”, these resists are designed such that, upon exposure, they can be selectively etched in either the exposed or unexposed regions by plasma techniques (178–180).

Ion bombardment can be used to enhance resist etch rates and thus achieve anisotropic resist profiles. Reactive sites produced by bombardment permit more rapid attack by oxygen species in the plasma. Multilevel processing (181, 182), in which an etch-resistant layer serves as a mask to pattern

a polymer or other planarizing film, relies heavily on such anisotropic resist development (183). This approach can be implemented by using a thin organic resist on top of the masking layer (trilevel process) or by combining the function of the resist layer with the intermediate (masking) layer (bilevel process). In the bilevel process, silicon-containing resists such as polysilanes and polysiloxanes have been used (184). Alternatively, a resist can be exposed but functionalized prior to development. The functionalization involves selective incorporation (because of different reactivities) of a silicon-containing vapor such as hexamethyldisilazane into the exposed resist areas (185).

Ultraviolet light, which is present in all glow discharges, also enhances the purely chemical etchant activity and is particularly important for organic film materials. The photochemistry of organic molecules is a well-established field (186). Although polymeric films are a more complex photochemical system, many of the chromophoric groups in the polymer react similarly under exposure to UV radiation. The most serious degradation results when scission of backbone or side-chain (near the backbone) bonds of the polymer occurs. The predominant degradation mechanism in polymers exposed to plasma environments is random chain scission (187). Active sites then become available for reaction with atomic and molecular species in the plasma. To stabilize these bonds, polymer scientists design side groups far removed from the backbone to reduce the impact of photochemical attack on the polymer chain.

After the resist has served its purpose as an etch mask, it must be removed prior to subsequent processing. Exposure to plasma atmospheres (or ion implantation) often renders the resist material impervious to complete removal by liquid etch baths. As a result, glow discharge methods are invoked to strip resists. With these methods, the most important criteria are etch rate and the minimization of radiation damage to or attack of underlying films or substrates. Etch rates are typically low in O₂ plasmas unless ion bombardment or elevated temperatures (>150 °C) are used, and recent efforts have concentrated on downstream reactors using microwave source gas (O₂ or O₂-CF₄) excitation (188–190). This configuration takes advantage of the efficiency of microwave generation of atoms and radicals, as well as the controlled rise in substrate temperature without high-energy-particle bombardment. These effects can lead to high resist stripping rates with little or no radiation damage. However, device degradation can still occur if contaminants (e.g., iron or lead) are present in the resist. These species are diffused into SiO₂ surfaces at elevated temperatures (>150 °C) even during downstream stripping (191).

Profile Control

The goal of any pattern-etching process is to transfer an exact replica of the mask features to the underlying film. However, this transfer establishes only

a two-dimensional criterion for the quality of the replication. The third dimension relates to the cross section or edge profile of the etched feature (2, 192).

The simplest and perhaps the most useful measure of anisotropy is the ratio of lateral or horizontal undercut distance (d_h) to the vertical etch distance (d_v). This ratio is inversely related to the quality of replication. In anisotropic etching, $d_h/d_v = 0$, and exact dimensional transfer is achieved. A low-quality transfer is obtained with isotropic etching, in which $d_h/d_v = 1$. Anisotropic etching is imperative for high-density-device fabrication.

The desired edge profile depends upon the specific application of the film in the final device. For instance, if a metal line is being defined, a steep-walled profile is desirable to maximize the conductor cross-sectional area. Anisotropic etching can yield such profiles with line dimensions of $\sim 0.1 \mu\text{m}$. However, if good step coverage is desired, a tapered or sloped profile is required so that subsequent film deposition will uniformly cover the step, that is, without thinning of the film because of shadowing during deposition. Some control of the taper can be achieved by the proper choice of resist process and plasma conditions. If isotropic etching is needed, for example, to clean the side walls after a sputter etch (physical ablation of material) or to produce a slight undercut, a purely chemical etch process is required.

Isotropic etching is achieved by using a barrel reactor with an etch tunnel or, better yet, with a downstream reactor configuration so that radiation bombardment of etching surfaces is eliminated (193, 194). Anisotropic or directional etching (in which the taper is 90° or less) can be achieved in several ways. Sputtering generates a high degree of anisotropy because of the directional nature of the inert gas ions that physically ablate (via momentum transfer) the film material. However, sputter etching (94, 192) redeposits etched material, is only weakly selective, and exhibits low etch rates. Ion bombardment in the presence of chemically reactive species (plasma etching) can alleviate these problems by forming volatile etch products, invoking chemical reactions for specificity, and taking advantage of the density of highly reactive neutral species in glow discharges. Although a fundamental understanding of the generation of anisotropic profiles has not been established (*see Synergistic Phenomena*), phenomenological models that present guidelines for variations in anisotropic edge profiles do exist (94, 99, 195).

Ion bombardment promotes surface bond breaking (*see Synergistic Phenomena*) and causes sputtering; therefore, etch rates are generally enhanced where bombardment occurs. Qualitatively, these phenomena can lead to anisotropy in two ways (94, 95, 105, 195), as depicted in Figure 10 (94). In the ion-induced-damage mechanism, energetic ions break chemical bonds on the film surface, thereby making the film more re-

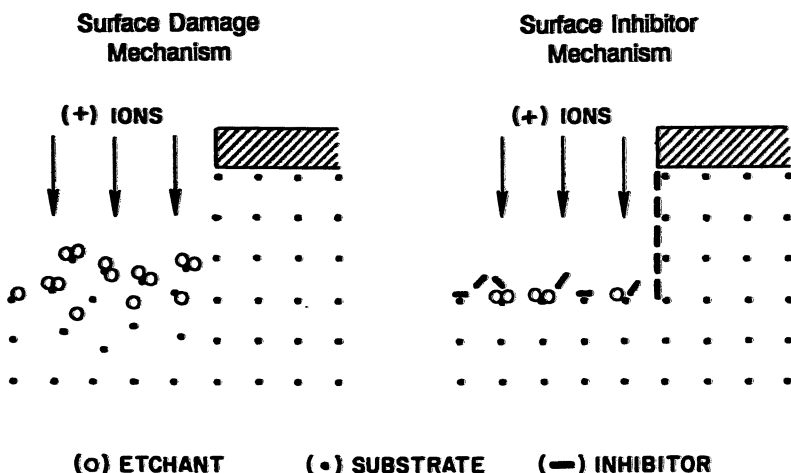


Figure 10. Surface damage and surface inhibitor mechanisms for ion-assisted anisotropic etching. (Reproduced with permission from reference 94. Copyright 1981 Plenum Publishing Corporation.)

active to chemical etchant species. However, the side walls remain relatively unperturbed, because ions primarily impinge perpendicularly to the film surface. Thus, etching proceeds at the nominal chemical etch rate. Material removal is more rapid in the direction of the ion flux and results in anisotropy.

In actual fact, the surfaces exposed to the plasma are usually composed of a chemisorbed coating of etchant radicals, as well as unsaturated species and resist fragments that inhibit the etch rate. Ion bombardment can stimulate the desorption of these species so that surface coverage caused by inhibitors is smallest in regions of high ion flux (Figure 10). Again, increased anisotropy is the net result. The ion-induced-damage mechanism requires considerably more energy than the surface inhibitor mechanism for anisotropy, and both are likely to play a role in plasma-etching processes. The degree of anisotropy will depend on ion flux, ion energy, and chemistry in the plasma.

As noted earlier, ion flux, energy, and plasma chemistry depend strongly on reactor design and gas composition and are therefore virtually impossible to translate directly from one reactor to another. Such possibilities await the development of accurate plasma models (*see* Modeling Plasma Processes). However, the important parameters can be identified to some extent. Ion bombardment is enhanced by decreasing pressure in a high-frequency plasma (~5 MHz) or by decreasing the frequency of the plasma discharge (22); anisotropic profiles thereby result (196). Anisotropies induced by surface damage and surface inhibitor (from photoresist as well as other fragments)

are possible; however, as pressure increases and ion energies become moderate because of collisions, the inhibitor mechanism becomes more favorable. Under these conditions, anisotropy can be achieved by adding film-forming precursors (CHF_3 , C_2H_2 , C_2F_6 , etc.) to the plasma (105, 197). At low frequencies (1 kHz–1 MHz), ions are strongly accelerated because of the longer duration of the accelerating potential, and both anisotropic mechanisms operate at much higher gas pressures. Even at high pressures (133 Pa) and frequencies, however, anisotropy can be achieved if the electric field across the sheath is sufficiently large (198).

An interesting demonstration of profile control via alteration of the specific chemistry is that of silicon etching in ClF_3 mixtures (86). Because a pure chemical (isotropic) etchant (F atoms) is combined with an ion-bombardment-controlled (anisotropic) etchant (Cl atoms), a continuous spectrum of profiles with varying anisotropies is generated by changing the gas composition.

Etch profiles can also be altered by controlling the susceptibility to erosion of the masking layer as shown in Figure 11 (199). If a masking layer that does not erode is used (e.g., MgO and Al_2O_3), a vertical (perfectly anisotropic) etch profile results. However, if the masking layer is attacked by chemical reaction or physical ablation (e.g., organic resist materials), the edges of the layer at the opening are removed. This removal exposes the edges of the underlying film to the plasma atmosphere. Further removal of the resist exposes additional film surface for etching. In this way, a tapered profile can be achieved. Such procedures require close control of resist processes as well as plasma conditions.

Deposition of Specific Film Materials

Like the literature of plasma-assisted etching, the literature on the PECVD of specific materials is considerable. Because film properties are ultimately determined by chemical reaction mechanisms, reactor design, and film structure (Figure 5), the determination of the exact relationships between properties and processing is difficult. At present, the fundamental understanding of such relationships is limited, and thus, empirical efforts have been the norm. In this chapter, the more widely studied film materials deposited by PECVD will be briefly discussed. More extensive information on these and other films can be found in a number of review articles (9–14, 32, 50, 200–203) and references therein.

Silicon. The most widely studied and perhaps the best understood PECVD film is that of amorphous silicon (a-Si). Glow discharge a-Si is an “alloy” of silicon and hydrogen, with the hydrogen content ranging from ~5 to 35 atom percent (atom %), depending upon the deposition conditions (temperature, rf power, rf frequency, etc.) and the resulting film structure.

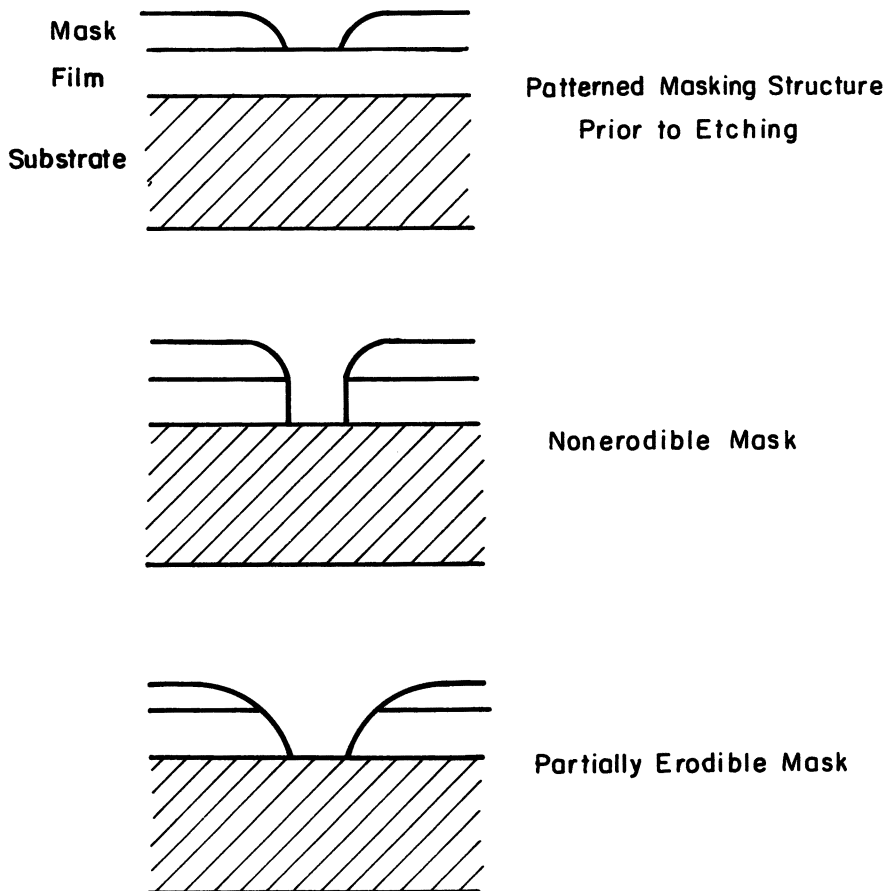


Figure 11. Schematic diagram comparing the control of etch profiles by the use of erodible and nonerodible mask materials. (Reproduced with permission from reference 199. Copyright 1980 John Wiley.)

The great interest in this material stems from its applications in solar-energy conversion, thin-film transistors, memory switches, and electrophotography (204).

Although the production of a-Si from SiH_4 (or from mixtures of SiH_4 with inert gases or H_2) is chemically one of the simplest reactions imaginable, the fundamental reactions involved in film formation and the structure–property relationships are not yet clearly defined (70, 200, 205–207). In particular, the role of hydrogen in film structure is complex and involves the reduction of silicon dangling bonds that degrade device properties. Infrared (208) and nuclear magnetic resonance (NMR) (209) spectra of deposited films have established that hydrogen exists in several bonding configurations: monohydride ($\equiv\text{Si}-\text{H}$), dihydride ($=\text{SiH}_2$), trihydride ($-\text{SiH}_3$), and poly-

meric ($-\text{SiH}_2-$)_n. Furthermore, NMR studies have suggested that Si–H can be randomly distributed or clustered in the structure (207, 209).

For the most part, even qualitative relationships between such structural considerations and film properties are lacking. Recently, however, two important correlations have been presented: Device quality a-Si contains only monohydride bonding structures (207), and the intrinsic film stress rises drastically as a morphological transition from columnar to noncolumnar growth occurs (210). Both studies point to the importance of defects in a-Si, although the precise role of these defects is still unclear.

The gas-phase and surface reactions in a-Si deposition by PECVD are equally nebulous. Reactive species, primarily H, SiH, SiH₂, SiH₃, and their positive ions (70, 205, 206), are produced by electron-impact decomposition of silane. Secondary reactions between these precursors to form species such as disilane (Si₂H₆) and higher molecular weight compounds are important in establishing reactive-species concentrations. Laser-light-scattering studies suggest that particle growth occurs in the plasma near the sheath edges (211, 212). Radicals, atoms, and ions diffuse or drift to the growing film surface, where they are adsorbed and undergo various reactions yielding solid and gaseous (e.g., SiH₄, Si₂H₆, and H₂) products. The surface reactions are generally modified by ion and photon bombardment. Adsorption sites can be created by bond breaking due to ion impingement or by atom (e.g., H) abstraction due to reaction with H atoms, SiH₂, or SiH₃ from the gas phase. Finally, bond rearrangement and an increase in film density due to loss of hydrogen occur.

Polycrystalline silicon (poly-Si) has been formed by the plasma-enhanced decomposition of dichlorosilane in argon at temperatures above 625 °C, a frequency of 450 kHz, and a total pressure of 27 Pa. Doped films have been deposited by the addition of phosphine to the deposition atmospheres (213). Approximately 1 atom % of chlorine was found in the as-deposited films. Annealing in nitrogen at temperatures above ~750 °C caused chlorine to diffuse from the film surface, grain growth to occur, and the film resistivity to drop. Such heat treatments were necessary to achieve integrated-circuit-quality films.

The drive to reduce process temperatures has led to an interest in growing epitaxial (crystalline) silicon films at temperatures below 800 °C. In addition to increasing deposition rates, glow discharges can assist surface cleaning so that epitaxy can be achieved. Indeed, crystalline silicon films have been produced by PECVD from SiH₄ atmospheres by using external coil excitation (214) or by downstream configurations (215, 216). In all cases, in situ surface cleaning, including the removal of the native silicon oxide layer, was imperative for epitaxy. If adequate cleaning (usually by ion bombardment) is performed, crystalline layers of silicon can be grown by low-pressure CVD, albeit with a low deposition rate (relative to that of PECVD). Thus, the primary role of a plasma in epitaxial growth may be surface cleaning, in addition to enhancement of reaction kinetics.

Silicon Nitride. Silicon nitride produced by high-temperature ($>700^{\circ}\text{C}$) CVD is a dense, stable, adherent dielectric that is useful as a passivation or protective coating, interlevel metal dielectric layer, and antireflection coating in solar cells and photodetectors. However, these applications often demand low deposition temperatures ($<400^{\circ}\text{C}$) so that low-melting-point substrates or films (e.g., Al or polymers) can be coated. Therefore, considerable effort has been expended to form high-quality silicon nitride films by PECVD.

A critical aspect of silicon nitride deposition by PECVD is that a significant concentration of hydrogen ($>10^{21}/\text{cm}^3$) is present in the deposited films (217–223). For this reason, silicon nitride will be referred to as SiN_xH_y . The hydrogen originates from SiH_4 or NH_3 , the typical reactants for PECVD. For the most part, hydrogen is bonded to either silicon (~75%) or nitrogen (~25%) (217, 218, 220, 223). The exact concentration and chemical distribution of hydrogen greatly affect film properties such as refractive index, etch rate, optical absorption edge, stress, and electrical conductivity. The concentrations and bonding configurations of Si, N, and H depend upon deposition and plasma conditions such as pressure, reactant ratio, rf power, rf frequency, and substrate temperature (217–224). In addition, rearrangement of hydrogen bonds in the film or diffusion of hydrogen out of the film can cause instabilities in devices fabricated with SiN_xH_y (225, 226).

In general, an increase in rf power density decreases the Si/N ratio in the film (227–229). Because the binding energy of the Si–H bond is less than those of the N–H and N–N bonds, an increase in rf power should increase the concentration of reactive nitrogen species relative to the number of reactive silicon species and thereby decrease the Si/H ratio in the film. At high power densities and at high temperatures, the Si/N ratio approaches 0.75, which is the stoichiometric ratio for Si_3N_4 .

Much of the data on film etch rate, density, refractive index, and conductivity can be correlated to the concentration and bonding configuration of hydrogen in the films. The total hydrogen concentration decreases with increasing temperature and decreasing frequency (219, 221, 227, 230, 231). With increasing substrate temperature, adsorbed surface species have more energy, can preferentially form Si–N bonds, and thereby release hydrogen. Similar effects are operative at low frequency (<4 MHz), where adatom mobility and hydrogen removal by sputtering are favored. The correlation between the effects of deposition temperature and ion bombardment in SiN_xH_y is shown in Figure 12 (221). When adequate thermal energy is available (deposition temperature $>300^{\circ}\text{C}$), the total hydrogen content in the film is controlled by thermally activated desorption. Below 300°C , the hydrogen concentration is determined by ion bombardment.

The hydrogen content of SiN_xH_y produced by PECVD can be reduced but not eliminated in several ways. The use of N_2 rather than NH_3 as the

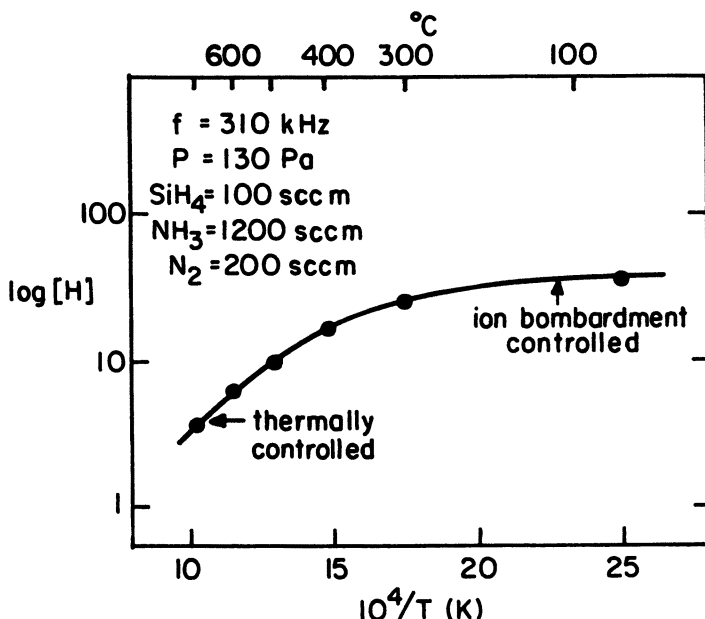


Figure 12. Hydrogen concentration versus temperature for silicon nitride layers deposited by PECVD. (sccm is standard cubic centimeters per minute.) (Reproduced with permission from reference 221. Copyright 1985 The Electrochemical Society, Inc.)

nitrogen source reduces the amount of H in the film, but difficulty is often encountered with silicon-rich films because of the strong N–N bond (232). Even with N_2 , high temperatures and power levels are needed to effectively minimize H (228). Hydrogen can also be scavenged by incorporating a fluorine-containing reactant so that H content is reduced by formation of HF that is removed from the chamber. However, when SiF_4 or SiF_2 is used as a reactant with N_2 – H_2 mixtures, large concentrations of fluorine (10–25 atom %) are incorporated into the films (233). The Si–F bonds in such films can hydrolyze upon postdeposition exposure to air (234) to form silicon oxynitride films.

An alternative but effective way to scavenge hydrogen is to use NF_3 – NH_3 mixtures as the nitrogen source (234). With this nitrogen source, lower concentrations of F (<8 atom %) can be incorporated in the films by altering the NF_3/NH_3 ratio. Finally, the use of downstream PECVD in which only NH_3 –He or NH_3 –Ar mixtures are plasma excited has shown promise in minimizing the formation of Si–H bonds (or N–H bonds with N_2 –He mixtures) (50).

Hydrogen is not the only impurity frequently incorporated into SiN_xH_y films produced by PECVD. Oxygen is generally found in the films and is believed to come from desorbed water vapor from reactor walls or from small

vacuum system leaks. Even small quantities of oxygen reduce the refractive index, increase the etch rate, and decrease the film stress (221, 235).

SiN_xH_y can be deposited by PECVD with either a compressive or a tensile stress, depending upon the deposition conditions. Although rf power, pressure, and temperature affect stress, rf frequency is a critical parameter at low temperatures ($<300\text{ }^\circ\text{C}$) (221, 236). At low frequencies ($<4\text{ MHz}$), the stress is generally compressive, whereas at higher frequencies (especially at elevated pressures), tensile stress is often observed. Upon postdeposition, high-temperature ($>500\text{ }^\circ\text{C}$) heat treatments, the stress varies inversely with hydrogen concentration; in this study (221), the stress was independent of Si–H content but increased linearly with decreasing N–H concentration. If the stress level of SiN_xH_y deposited by PECVD is too high, the films crack either during or after deposition or after subsequent heat treatments (235, 237). Film stress can significantly affect adhesion.

Silicon Dioxide. SiO_2 layers produced by PECVD are useful for intermetal dielectric layers and mechanical or chemical protection and as diffusion masks and gate oxides on compound-semiconductor devices. The films are generally formed by the plasma-enhanced reaction of SiH_4 at 200–300 $^\circ\text{C}$ with nitrous oxide (N_2O), but CO, CO_2 , or O_2 have also been used (238–241). Other silicon sources including tetramethoxysilane, methyl dimethoxysilane, and tetramethylsilane have also been investigated (202). Diborane or phosphine can be added to the deposition atmosphere to form doped oxide layers.

Like SiN_xH_y deposited by PECVD, SiO_2 films deposited by PECVD contain hydrogen (203, 240, 242). Because of the enhanced reactivity of oxygen with SiH_4 fragments compared with nitrogen species, lower concentrations of hydrogen are present in SiO_2 (2–9 atom %) than in SiN_xH_y (15–30 atom %) films. The primary bonding configurations for H are SiH, SiOH, and H_2O (240, 242). The distribution of hydrogen between these moieties depends upon deposition conditions. The electrical properties of SiO_2 films are improved if SiOH bonds are minimized (203). Because of the use of N_2O , a small amount of N (<5 atom %) is also incorporated into the deposited films.

The properties of silicon dioxide films also depend upon all plasma deposition parameters. Temperature is the critical parameter (240), although the compressive stress level varies with rf frequency (237, 240). Film topography can be varied during deposition by altering ion bombardment conditions (242, 243). In particular, the incorporation of Ar in the deposition atmosphere enhances sputtering and thus promotes conformal step coverage during film formation (243).

Conducting Films. To improve adhesion, grain structure, and step coverage of metal films at low temperatures, much interest has been centered

recently in PECVD. One of the major limitations of this approach to metal deposition is the availability of suitable source vapors. Generally, reactant species are halides, carbonyls, or alkyls. In the reactive plasma atmosphere, halogens, carbon, or oxygen are therefore often incorporated into the deposited film. Because metallic-film properties are highly sensitive to small concentrations of impurities present in the film, the incorporation of these atoms, as well as oxygen from leaks and chamber outgassing, must be minimized in order to produce low-resistivity films. In addition, the halogen atoms are often etchants for the depositing film material. This situation results in a dynamic equilibrium between etching and deposition so that deposition rates may be low. Nevertheless, a number of film materials have been formed, albeit generally with higher than bulk (or even evaporated, sputtered, or deposited by CVD) resistivities. In certain cases, the elevated resistivities may also be due to metastable-phase formation (244). A summary of these film materials, their deposition conditions, and their resistivities is shown in Table V (201, 245–253).

Carbon. Carbon films have recently generated considerable interest because of their potentially useful properties: electrical insulation, thermal conductivity, optical transparency, chemical resistance, and mechanical hardness. Much of the effort has centered around amorphous carbon (a-C), which is a metastable phase of carbon that contains hydrogen and displays properties that are intermediate between those of graphite and diamond (254–256). Numerous hydrocarbons have been used as source gases, including methane, acetylene, ethylene, propane, butane, and benzene (254–259). Although these films are often referred to as diamond-like, at least at PECVD deposition temperatures below ~400 °C, at least one hydrogen is bonded to each carbon atom (256). At ~425 °C, deposited films have properties similar to those of graphite, a fact suggesting that a-C is metastable with respect to graphite, perhaps because of the removal of

Table V. Summary of Conducting Films Deposited in rf Glow Discharges

<i>Film</i>	<i>Reactants</i>	<i>Electrode Temperature</i> (°C)	<i>Pressure</i> (Pascal)	<i>Frequency</i> (MHz)	<i>As-Deposited Sheet Resistivity</i> (Ω/\square) ^a		<i>Reference</i>
					<i>Resistivity</i> (Ω/\square) ^a	<i>Reference</i>	
W	WF ₆ + H ₂	350	27	4.5	2	246	
Mo	MoF ₆ + H ₂	350	27	4.5	400	246	
	MoCl ₅ + H ₂	430	—	—	(500)	247	
WSi _x	WF ₆ + SiH ₄	230	80	13.56	(~500)	248	
MoSi _x	MoCl ₅ + SiH ₄	400	—	—	(800)	247	
TiSi _x	TiCl ₄ + SiH ₄	450	267	0.05	15–20	249	
	TiSi _x + SiH ₄	350	133	0.3	—	250	
TaSi _x	TaCl ₅ + SiH ₄ Cl ₂ + H ₂	650	200	0.6	(70)	251	
TiN _x	TiCl ₄ + NH ₃ + H ₂	600	27	13.56	30	252	
TiB _x	TiCl ₄ + BCl ₃ + H ₂	600	40	15	(200)	253	

^aNumbers in parentheses are resistivities in microohm-centimeter.

hydrogen with the subsequent collapse of the C–H structure (256). Polycrystalline and crystalline diamond films have been formed (260–262), although the exact nature of the reactions needed to form crystallites is not yet clear. Theories include hydrogen atom generation or the specific energy of certain plasma-excited hydrocarbon fragments.

Summary and Conclusions

Glow discharges or plasmas have been used extensively to promote chemical reactions for thin-film etching and deposition in a variety of technologically important areas. The reactive chemical atmosphere and complex discharge–surface interactions in these systems permit the attainment of unique etch profiles and film properties.

At present, reproducibility and control are the primary limitations to the implementation of plasma processes; clearly, the large number of interacting parameters accounts for such problems. In addition, deposition and etching processes are inordinately sensitive to small (part-per-billion) concentrations of impurities. These difficulties can be overcome only by careful investigation of the complex chemistry and physics of glow discharges.

Much progress has been made in recent years. Many of the required gas-phase parameters (reaction rates, cross sections, species concentrations, etc.) can be measured, even though the necessary attempts have not been mounted in all cases.

The principal impediment to effective process design and analysis is the limited understanding of synergistic effects due to ion, photon, and electron bombardment of solid surfaces during etching and deposition. Fundamental relationships must be established between the gas-phase chemistry; the surface chemistry as modified by radiation; and etch profiles, rates, selectivities, and film properties.

This lack of fundamental understanding of the science and engineering of plasma processing is reminiscent of the situation in the catalytic field a few decades ago. With the proper research efforts in surface- and gas-phase chemistry, engineering, and reactor design, most of the current problems can be overcome, and the ultimate capabilities of plasma processing can be realized.

References

1. Kern, W.; Deckert, C. A. In *Thin Film Processes*; Vossen, J. L.; Kern, W., Eds.; Academic: New York, 1978; p 401.
2. Mucha, J. A.; Hess, D. W. In *Introduction to Microlithography*; Thompson, L. F.; Willson, C. G.; Bowden, M. J., Eds.; ACS Symposium Series 219; American Chemical Society: Washington, DC, 1983; p 215.
3. Flamm, D. L.; Donnelly, V. M.; Ibbotson, D. E. In *VLSI Electronics: Microstructure Science*; Einspruch, N. G.; Brown, D. M., Eds.; Academic: New York, 1984; Vol. 8, p 189.

4. Smith, D. L. In *VLSI Electronics: Microstructure Science*; Einspruch, N. G.; Brown, D. M., Eds.; Academic: New York, 1984; Vol. 8, p 253.
5. Goworwitz, B.; Saia, R. J. In *VLSI Electronics: Microstructure Science*; Einspruch, N. G.; Brown, D. M., Eds.; Academic: New York 1984; Vol. 8, p 297.
6. *Dry Etching for Microelectronics*; Powell, R. A., Ed.; North-Holland: Amsterdam, 1984.
7. *Handbook of Thin Film Technology*; Maissel L. I.; Glang, R., Eds.; McGraw-Hill, New York, 1970.
8. Vossen, J. L.; Kern, W. *Thin Film Processes*; Academic: New York, 1978.
9. *Deposition Technologies for Films and Coatings*; Bunshah, R. F., Ed.; Noyes: Park Ridge, NJ, 1982.
10. Ojha, S. M. In *Physics of Thin Films*; Haas, G.; Francombe, M. H.; Vossen, J. L., Eds.; Academic: New York, 1982; p 237.
11. Thornton, J. A. *Thin Solid Films* 1983, 107, 3.
12. Hess, D. W. *J. Vac. Sci. Technol., A* 1984, 2, 244.
13. Reif, R. *J. Vac. Sci. Technol., A* 1984, 2, 429.
14. Catherine, Y. In *Plasma Processing*; Mathad, G. S.; Schwartz, G. C.; Smolinsky, G., Eds.; Electrochemical Society: Pennington, 1985; p 317.
15. Bell, A. T. In *Techniques and Applications of Plasma Chemistry*; Hollahan, J. R.; Bell, A. T., Eds.; Wiley: New York, 1974; p 1.
16. Vossen, V. L. *J. Electrochem. Soc.* 1979, 126, 319.
17. Chapman, B. N. *Glow Discharge Processes*; Wiley: New York, 1980.
18. Butler, H. S.; Kino, G. S. *Phys. Fluids* 1963, 6, 1346.
19. a. Anderson, G. S.; Mayer, W. B.; Wehner, G. K. *J. Appl. Phys.* 1962, 33, 2991. b. Gottscho, R. A.; Gaebe, C. E. *IEEE Trans. Plasma Sci.* 1986, PS-14, 92.
20. Koenig, H. R.; Maissel, L. I. *IBM Res. Dev.* 1970, 14, 168.
21. Coburn, J. W.; Kay, E. *J. Appl. Phys.* 1972, 43, 4965.
22. Bruce, R. H. *J. Appl. Phys.* 1981, 52, 7064.
23. Winters, H. F. In *Plasma Chemistry III*; Veprek S.; Venugopalan M., Eds.; Springer-Verlag: New York, 1980; p 69.
24. Bell, A. T. *Solid State Technol.* 1978, 214, 89.
25. McDaniel, E. W. *Collision Phenomena In Ionized Gases*; Wiley: New York, 1964.
26. Massey, H. S. W.; Burhop, E. H. S.; Gilbody, H. B. *Electronic and Ionic Impact Phenomena*; Oxford: New York, 1971.
27. McDavid, E. W.; Cermak, V.; Dalgarno, A.; Ferguson, E. E.; Friedman, L. *Ion-Molecule Reactions*; Wiley: New York, 1970.
28. Kondratiev, V. N. *Chemical Kinetics of Gas Reactions*; Addison-Wesley: Boston, 1964.
29. Muschitz, E. E., Jr. *Science (Washington, D.C.)* 1968, 159, 599.
30. Carter, G.; Colligan, J. S. *Ion Bombardment of Solids*; Elsevier: New York, 1969.
31. *Ion Bombardment Modification of Surfaces*; Aucellio, O.; Kelly, R., Eds.; Elsevier: Amsterdam, 1984.
32. Hess, D. W. *Annu. Rev. Mat. Sci.* 1986, 16, 163.
33. Gerlach-Meyer, U.; Coburn, J. W.; Kay, E. *Surf. Sci.* 1981, 103, 177.
34. Hagstrum, H. D. *Phys. Rev.* 1961, 396, 36.
35. Greene, J. E.; Barrett, S. A. *J. Vac. Sci. Technol.* 1982, 21, 285.
36. Takagi, T. *J. Vac. Sci. Technol., A* 1984, 2, 382.
37. Donnelly, V. M.; Flamm, D. L. *Solid State Technol.* 1981, 244, 161.
38. Coburn, J. W. In *Proceedings of the Tutorial Symposium on Semiconductor Technology*; Doane, D. A.; Fraser, D. B.; D. W. Hess, Eds.; Electrochemical Society: Pennington, 1982; p 177.

39. Coburn, J. W.; Winters, H. F. *J. Appl. Phys.* **1979**, *50*, 3189.
40. Kay, E.; Coburn, J. W.; Dilks, A. In *Plasma Chemistry III*; Veprek, V.; Venugopalan, V., Eds.; Springer-Verlag: New York, 1980; p 1.
41. Frieser, R. G.; Montillo, F. J.; Zingerman, N. B.; Chu, W. K.; Mader, S. R. *J. Electrochem. Soc.* **1983**, *130*, 2237.
42. a. Pang, S. *Solid State Technol.* **1984**, *274*, 249. b. Fonash, S. J. *Solid State Technol.* **1985**, *284*, 201.
43. Oehrlein, G. S.; Tromp, R. M.; Tsang, J. C.; Lee, Y. H.; Petrillo, E. J. *J. Electrochem. Soc.* **1985**, *132*, 1441.
44. Ryden, K.-H.; Norstrom, H.; Nender, C.; Berg, S. J. *J. Electrochem. Soc.* **1987**, *134*, 3113.
45. Dautremont-Smith, W. C.; Feldman, L. C. *J. Vac. Sci. Technol., A* **1985**, *3*, 873.
46. Hess, D. W. In *Silicon Processing*; Gupta, D. C., Ed.; Am. Soc. Testing and Materials: Washington, DC, 1983; p 218.
47. Bondur, J. A. *J. Vac. Sci. Technol.* **1978**, *13*, 1023.
48. Lehmann, H. W.; Widmer, R. *J. Vac. Sci. Technol.* **1978**, *15*, 319.
49. Meiners, L. G. *J. Vac. Sci. Technol.* **1982**, *21*, 655.
50. Lucovsky, G.; Tsu, D. V.; Markunas, R. J. In *Plasma Processing*; Coburn, J. W.; Gottscho, R. A.; Hess, D. W., Eds.; Materials Research Society: Pittsburgh, 1986; Vol. 68, p 323.
51. Horiike, Y.; Shibagaki, M. In *Semiconductor Silicon 1977*; Huff, H. R.; Sirtl, E., Eds.; Electrochemical Society: Pennington, 1977; p 1071.
52. Spencer, J. E.; Borel, R. A.; Hoff, A. *J. Electrochem. Soc.* **1986**, *133*, 1922.
53. von Engel, A. *Ionized Gases*; Oxford University Press: London, 1965.
54. Pitchford, L. C.; O'Neil, S. V.; Rumble, J. R. *Phys. Rev.* **1981**, *23*, 294.
55. Winkler, R.; Deutsch, H.; Wilhelm, J.; Wilke, C. *Beitr. Plasmaphys.* **1984**, *243*, 285–316.
56. Kitamori, K.; Tagashira, H.; Sakai, Y. *J. Phys. D* **1980**, *13*, 535.
57. Penetrante, B. M.; Bardsley, J. N. *J. Phys. D* **1984**, *17*, 1971.
58. Hunter, S. R. *Austr. J. Phys.* **1977**, *30*, 83.
59. Blevin, H. A.; Fletcher, J.; Hunter, S. R. *Austr. J. Phys.* **1978**, *31*, 299.
60. Coltrin, M. E.; Kee, R. J.; Miller, J. A. *J. Electrochem. Soc.* **1984**, *131*, 425.
61. Wahl, G. *Thin Solid Films* **1977**, *40*, 13.
62. Gottscho, R. A.; Miller, T. A. *Pure Appl. Chem.* **1984**, *56*, 189.
63. *Combustion Chemistry*; Gardiner, W. C., Ed.; Springer-Verlag, New York, 1984.
64. Hess, D. W.; Jensen, K. F.; Anderson, T. J. *Rev. Chem. Eng.* **1985**, *3*, 97.
65. Jensen, R. J.; Bell, A. T.; Soong, D. S. *Plasma Chem. Plasma Proc.* **1983**, *3*, 163.
66. a. Graves, D. B. In *Plasma Processing*; Mathad, G. S.; Schwartz, G. C.; Gottscho, R. A., Eds.; Electrochemical Society: Pennington, 1987; p 267. b. Boeuf, J. P. *Phys. Rev. A* **1987**, *36*, 2782. c. Barnes, M. S.; Cotler, T. J.; Elta, M. E. *J. Appl. Phys.* **1987**, *61*, 81. d. Richards, A. D.; Thompson, B. E.; Sawin, H. H. *Appl. Phys. Lett.* **1987**, *50*, 492.
67. Bell, A. T. *I&EC Fundamentals* **1970**, *9*, 160.
68. Brown, L. C.; Bell, A. T. *I&EC Fundamentals* **1970**, *13*, 210.
69. Bell, A. T.; Kwong, K. *AICHE J.* **1972**, *18*, 990.
70. Turban, G.; Catherine, Y.; Grolleau, B. *Plasma Chem. Plasma Proc.* **1982**, *2*, 61.
71. Turban, G.; Catherine, Y.; Grolleau, B. *Thin Solid Films* **1979**, *60*, 147.
72. Turban, G.; Catherine, Y. *Thin Solid Films* **1978**, *48*, 57.
73. Chen, I. *Thin Solid Films* **1983**, *101*, 41.

74. Winters, H. F.; Coburn, J. W.; Kay, E. *J. Appl. Phys.* **1977**, *48*, 4973.
75. Kushner, M. *J. J. Appl. Phys.* **1982**, *53*, 2923.
76. Edelson, D.; Flamm, D. L. *J. Appl. Phys.* **1984**, *56*, 1522.
77. Kline, L. *IEEE Trans. Plasma Sci.* **1986**, *PS-14*, 145.
78. Anderson, H. M.; Merson, J. A.; Light, R. W. *IEEE Trans. Plasma Sci.* **1986**, *PS-14*, 156.
79. Kushner, M. J. *IEEE Trans. Plasma Sci.* **1986**, *PS-14*, 188.
80. Rhee, S.; Szekely, J. *J. Electrochem. Soc.* **1986**, *133*, 2194.
81. Greenberg, K. E.; Verdeyen, J. T. *J. Appl. Phys.* **1985**, *57*, 1596.
82. Tachibana, K.; Nishida, M.; Harima, H.; Urano, Y. *J. Phys. D* **1984**, *17*, 1727.
83. Alkire, R. C.; Economou, D. F. *J. Electrochem. Soc.* **1985**, *132*, 648.
84. Dalvie, M.; Jensen, K. F.; Graves, D. B. *Chem. Eng. Sci.* **1986**, *41*, 653.
85. Mogab, C. J. *J. Electrochem. Soc.* **1977**, *124*, 1262.
86. Flamm, D. L.; Wang, D. N.; Maydan, D. *J. Electrochem. Soc.* **1982**, *129*, 2755.
87. Marcoux, P. J.; Foo, P. W. *Solid State Technol.* **1981**, *244*, 115.
88. Dreyfus, R. W.; Jasinski, J. M.; Walkup, R. E.; Selwyn, G. S. *Pure Appl. Chem.* **1985**, *57*, 1265.
89. Roland, J. P.; Marcoux, P. J.; Ray, G. W.; Rankin, G. H. *J. Vac. Sci. Technol., A* **1985**, *3*, 631.
90. Bergeron, S. F.; Duncan, B. F. *Solid State Technol.* **1982**, *258*, 98.
91. Sawin, H. H.; Allen, K. D.; Jenkins, M. W. In *Eleventh Tegal Plasma Seminar Proceedings*, 1985; p 17.
92. Kay, E.; Coburn, J. W.; Dilks, In *Topics in Current Chemistry*; Veprek, S.; Venugopalan, M., Eds.; Springer-Verlag: New York, 1980; p 94, 1.
93. Flamm, D. L. *Plasma Chem. Plasma Proc.* **1981**, *1*, 37.
94. Flamm, D. L.; Donnelly, V. M. *Plasma Chem. Plasma Proc.* **1981**, *1*, 317.
95. Flamm, D. L.; Donnelly, V. M.; Mucha, J. A. *J. Appl. Phys.* **1981**, *52*, 3633.
96. Mogab, C. J.; Adams, A. C.; Flamm, D. L. *J. Appl. Phys.* **1979**, *49*, 3796.
97. Mucha, J. A.; Flamm, D. L.; Donnelly, V. M. *J. Appl. Phys.* **1982**, *53*, 4553.
98. Chuang, T. *J. J. Appl. Phys.* **1980**, *51*, 2614.
99. Flamm, D. L.; Donnelly, V. M.; Ibbotson, D. E. In *VLSI Electronics: Microstructure Science*; Einspruch, N. G.; Brown, D. M., Eds.; Academic: Orlando, FL, 1984; Vol. 8, p 189.
100. a. Stinespring, C. D.; Freedman, A. *Appl. Phys. Lett.* **1986**, *48*, 718. b. McFeely, F. R.; Morar, J. F.; Himpel, F. J. *Surf. Sci.* **1986**, *165*, 277.
101. d'Agostino, R.; Flamm, D. L. *J. Appl. Phys.* **1981**, *52*, 162.
102. Picard, A.; Turban, G. *Plasma Chem. Plasma Proc.* **1985**, *5*, 333.
103. a. Schwartz, G. C.; Schaible, P. M. *J. Vac. Sci. Technol.* **1979**, *16*, 410. b. Mogab, C. J.; Levenstein, H. J. *J. Vac. Sci. Technol.* **1980**, *17*, 721. c. Flamm, D. L.; Cowen, P. L.; Golovchenko, J. A. *J. Vac. Sci. Tech.* **1980**, *17*, 1341.
104. Chow, T. P.; Maciel, P. A.; Fanelli, G. M. *J. Electrochem. Soc.* **1987**, *134*, 1281.
105. Engelhardt, M.; Schwarzl, S. *J. Electrochem. Soc.* **1987**, *134*, 1985.
106. Adams, A. C.; Capio, C. D. *J. Electrochem. Soc.* **1981**, *128*, 366.
107. Barker, R. A.; Mayer, T. M.; Pearson, W. C. *J. Vac. Sci. Technol., B* **1983**, *1*, 37.
108. Sanders, F. H. M.; Kolfschoten, A. W.; Dieleman, J.; Haring, R. A.; de Vries, A. E. *J. Vac. Sci. Technol., A* **1984**, *2*, 487.
109. Rossen, R. A.; Sawin, H. H. *J. Vac. Sci. Technol., A* **1985**, *3*, 881.
110. McNevin, S. C.; Becker, G. E. *J. Vac. Sci. Technol., B* **1985**, *3*, 485.
111. Baldi, L.; Beards, D. *J. Appl. Phys.* **1985**, *57*, 2221.
112. Lee, Y. H.; Chen, M.-M. *J. Vac. Sci. Technol., B* **1986**, *4*, 468.

113. Heinicke, R. A. H. *Solid-State Electron.* 1975, 18, 1146; 1976, 19, 1039.
114. Clarke, P. E.; Field, D.; Hydes, A. J.; Klemperer, D. F.; Seakins, M. J. *J. Vac. Sci. Technol., B* 1985, 3, 1614.
115. Coburn, J. W.; Winters, H. F. *J. Vac. Sci. Technol.* 1979, 16, 391.
116. Turban, G.; Grolleau B.; Launay, P.; Briaud, P. *Rev. Appl. Phys.* 1985, 20, 609.
117. Coburn, J. W.; Winters, H. F. *Solid State Technol.* 1979, 224, 117.
118. Ephrath, L. M. *J. Electrochem. Soc.* 1979, 126, 1419.
119. Matsuo, S. *J. Vac. Sci. Technol.* 1980, 17, 587.
120. Mayer, T. M. *J. Electron. Mat.* 1980, 9, 513.
121. Toyoda, H.; Komiya, H.; Itakura, H. *J. Electron. Mat.* 1980, 9, 569.
122. Chang, R. H. P.; Chang, C. C.; Durack, S. *J. Vac. Sci. Technol.* 1982, 20, 45.
123. Klinger, R. E.; Greene, J. E. *J. Appl. Phys.* 1983, 54, 1595.
124. Smolinsky, S.; Chang, R. P. H.; Mayer, T. M. *J. Vac. Sci. Technol.* 1981, 18, 12.
125. Gottscho, R. A.; Smolinsky, G.; Burton, R. H. *J. Appl. Phys.* 1982, 53, 5908.
126. Stern, M. B.; Liao, P. F. *J. Vac. Sci. Technol., B* 1983, 1, 1053.
127. Ibbotson, D. E.; Flamm, D. L.; Donnelly, V. M. *J. Appl. Phys.* 1983, 54, 5974.
128. Li, J. Z.; Adesida, J.; Wolf, E. D. *J. Vac. Sci. Technol.* 1985, B3, 406.
129. Burton, R. H.; Gottscho, R. A.; Smolinsky, G. In *Dry Etching for Microelectronics*; Powell, R. A., Ed.; Elsevier: Amsterdam, 1984; p 79.
130. Hipwood, L. G.; Wood, P. N. *J. Vac. Sci. Technol., B* 1985, 3, 395.
131. Donnelly, V. M.; Flamm, D. L.; Collins, G. J. *J. Vac. Sci. Technol.* 1982, 21, 817.
132. Donnelly, V. M.; Flamm, D. L.; Tu, C. W.; Ibbotson, D. E. *J. Electrochem. Soc.* 1982, 129, 2533.
133. McNevin, S. C.; Becker, G. E. *J. Appl. Phys.* 1985, 58, 4670.
134. Hess, D. W.; Bruce, R. H. In *Dry Etching for Microelectronics*; Powell, R. A., Ed.; Elsevier: Amsterdam, 1984, p 1.
135. Schwartz, G. C. In *Plasma Processing*; Mathad, G. S.; Schwartz, G. C.; Smolinsky, G., Eds.; Electrochemical Society: Pennington, 1985; p 26.
136. Tokunaga, K.; Redeker, F. C.; Danner, D. A.; Hess, D. W. *J. Electrochem. Soc.* 1981, 128, 851.
137. Winkler, U.; Schmidt, F.; Hoffman, N. In *Plasma Processing*; Frieser, R. G.; Mobab, C. J., Eds.; Electrochemical Society: Pennington, 1981; p 253.
138. Herb, G. K.; Porter, R. A.; Cruzan, P. D.; Agraz-Guerena, K.; Soller, B. R. *Electrochem. Soc. Ext. Abstr.*, 1981, 81-2, 710.
139. Purdes, A. J. *J. Vac. Sci. Technol., A* 1983, 1, 712.
140. Schaible, P. M.; Metzger, W. C.; Anderson, J. P. *J. Vac. Sci. Technol.* 1978, 15, 334.
141. a. Keaton, A. L.; Hess, D. W. *J. Vac. Sci. Technol., A* 1985, 3, 962. b. Keaton, A. L.; Hess, D. W. *J. Appl. Phys.* 1988, 63, 533. c. Keaton, A. L.; Hess, D. W. *J. Vac. Sci. Technol., B* 1988, 6, 72. d. Bell, H. B.; Light, R. W.; Anderson, H. M. In *Plasma Processing*; Mathad, G. S.; Schwartz, G. C.; Gottscho, R. A., Eds.; Electrochemical Society: Pennington, 1987; p 35.
142. Poulsen, R. G.; Nentwich, H.; Ingrey, S. In Proc. of the Int. Elec. Dev. Mtg.; Washington, DC, 1976; p 205.
143. Smith, D. L.; Bruce, R. H. *J. Electrochem. Soc.* 1985, 129, 2045.
144. Danner, D. A.; Hess, D. W. *J. Electrochem. Soc.* 1986, 133, 151.
145. Danner, D. A.; Hess, D. W. *J. Appl. Phys.* 1986, 59, 940.
146. Winters, H. F. *J. Vac. Sci. Technol., B* 1985, 3, 9.
147. Lee, W. Y.; Eldridge, J. M.; Schwartz, G. C. *J. Appl. Phys.* 1981, 52, 2994.

148. Fok, Y. T. *Electrochem. Soc. Ext. Abstr.* 1980, 80-1, 301.
149. Hess, D. W. *Plasma Chem. Plasma Proc.* 1982, 2, 141.
150. Chow, T. P.; Saxena, A. N.; Ephrath, L. M.; Bennett, R. S. In *Dry Etching for Microelectronics*; Powell, R. A., Ed.; Elsevier: Amsterdam, 1984; p 9.
151. Chow, T. P.; Steckl, A. J. *J. Electrochem. Soc.* 1984, 131, 2325.
152. a. Tang, C. C.; Hess, D. W. *J. Electrochem. Soc.* 1984, 132, 115. b. Fischl, D. S.; Hess, D. W. *J. Electrochem. Soc.* 1987, 134, 2265. c. Hess, D. W. *Solid State Technol.* 1988, 314, 97.
153. Robb, F. Y. In *Plasma Processing*; Mathad, G. S., Schwartz, G. C.; Smolinsky, G., Eds.; Electrochemical Society: Pennington, 1985; p 1.
154. Mattausch, H. J.; Hasler, B.; Beinvogl, W. *J. Vac. Sci. Technol., B* 1983, 1, 15.
155. Cadieu, J. C.; Sivaram, S.; Reintsema, C. D. *J. Vac. Sci. Technol., A* 1986, 4, 739.
156. Legat, W. H.; Schilling, H. *Electrochem. Soc. Ext. Abstr.* 1975, 75-2, 336.
157. Poulsen, R. G. *J. Vac. Sci. Technol.* 1977, 14, 266.
158. Mogab, C. J.; Shankoff, T. A. *J. Electrochem. Soc.* 1977, 124, 1766.
159. Nakata, H.; Nishioka, K.; Abe, H. *J. Vac. Sci. Technol.* 1980, 17, 1351.
160. Harada, T.; Gamo, K.; Namba, S. *Jpn. J. Appl. Phys.* 1981, 20, 259.
161. Matsuo, S.; Takehara, Y. *Jpn. J. Appl. Phys.* 1977, 16, 175.
162. Lehmann, H. W.; Widmer, R. *Appl. Phys. Lett.* 1978, 32, 163.
163. Toyoda, H.; Komiya, H.; Itakura, H. *J. Electron. Mat.* 1980, 9, 569.
164. Taylor, G. N.; Wolf, T. M. *Polym. Eng. Sci.* 1980, 20, 1086.
165. Goldstein, I. S.; Kalk, F. J. *Vac. Sci. Technol.* 1981, 19, 743.
166. Turban, G.; Rapeaux, M. *J. Electrochem. Soc.* 1983, 130, 2231.
167. Lin, B. J. *J. Electrochem. Soc.* 1980, 127, 202.
168. Allen, R.; Foster, M.; Yen, Y.-T. *J. Electrochem. Soc.* 1982, 129, 1379.
169. Hiraoka, H.; Pacansky, J. *J. Electrochem. Soc.* 1981, 128, 2645.
170. Moran, J. M.; Taylor, G. N. *J. Vac. Sci. Technol.* 1981, 19, 1127.
171. Dobkin, D. M.; Cantos, B. D. *IEEE Electron Device Lett.* 1981, *EDL-2*, 222.
172. a. Cook, J. M.; Benson, B. W. *J. Electrochem. Soc.* 1983, 130, 2459. b. Cook, J. M. *Solid State Technol.* 1987, 304, 147.
173. Degenkolb, E. O.; Mogab, C. J.; Goldrick, M. R.; Griffiths, J. E. *Appl. Spectrosc.* 1976, 30, 520.
174. Stafford, B. B.; Gorin, G. J. *Solid State Technol.* 1977, 209, 51.
175. Reichelderfer, R. F.; Welty, J. M.; Battey, J. F. *J. Electrochem. Soc.* 1977, 124, 1926.
176. Szekeres, A.; Kirov, K.; Alexandrova, S. *Phys. Status Solidi A* 1981, 63, 371.
177. a. Kegel, B. *Circuits Mfg.* 1981, 21, 27. b. Rust, R. D.; Rhodes, R. J.; Parker, A. A. *Solid State Technol.* 1984, 274, 270. c. Lu, N. H.; Nielsen, C.; Welsh, J. A.; Babu, S. V.; Rembetski, J. F. In *Plasma Processing*; Mathad, G. S.; Schwartz, G. C.; Smolinsky, G., Eds.; Electrochemical Society: Pennington, 1985; p 175.
178. a. Taylor, G. N.; Wolf, T. M. *J. Electrochem. Soc.* 1980, 127, 2665. b. Taylor, G. N.; Wolf, T. M.; Moran, J. M. *J. Vac. Sci. Technol.* 1981, 19, 872.
179. Geis, M. W.; Randall, J. N.; Deutsch, T. F.; DeGraff, P. D.; Krohn, K. E.; Stern, L. A. *Appl. Phys. Lett.* 1983, 43, 74.
180. Hori, M.; Miwa, T.; Hattori, S.; Morita, S. *Plasma Chem. Plasma Proc.* 1984, 4, 119.
181. Lin, B. J. In *Introduction to Microlithography*; Thompson, L. F., Willson, C. G.; Bowden, M. J., Eds.; ACS Symposium Series 219; American Chemical Society: Washington, DC, 1983; p 287.
182. Kruger, J. B.; O'Toole, M. M.; Rissman, P. In *VLSI Electronic Microstructure*

- Science: *Plasma Processing for VLSI*; Einspruch, N. G.; Brown, D. M., Eds.; Academic: Orlando, FL, 1984; Vol. 8.
- 183. Chow, N. J.; Tang, C. H.; Paraszczak, J.; Babich, E. *Appl. Phys. Lett.* **1985**, *46*, 31.
 - 184. a. Hatzakis, M.; Paraszczak, J.; Shaw, J. In *Proc. Microcircuit Eng.* **81**; Lausanne, 1981. b. Saotome, Y.; Gokan, H.; Saigo, K.; Suzuki, M.; Ohnisihi, Y. *J. Electrochem. Soc.* **1985**, *132*, 919. c. Reichmanis, E.; Smolinsky, G.; Wilkins, C. W., Jr. *Solid State Technol.* **1985**, *288*, 130.
 - 185. a. Coopmans, F.; Roland, B. *SPIE Proc. Advances In Resist Technology III* **1986**, *633*, 126. b. Roland, B.; Lombaerts, R.; Jakus, C.; Coopmans, F. *SPIE Proc. Advances In Resist Technology IV*, **1988**, *771*, 69.
 - 186. Calvert, J. G.; Pitts, J. N., Jr. *Photochemistry*; Wiley: New York, 1967.
 - 187. Wu, B. J.; Hess, D. W.; Soong, D. S.; Bell, A. T. *J. Appl. Phys.* **1983**, *54*, 1725.
 - 188. Dzioba, S.; Este, G.; Naguib, H. M. *J. Electrochem. Soc.* **1982**, *129*, 2537.
 - 189. Charlet, B.; Peccoud, L. In *Plasma Processing*; Mathad, G. S.; Schwartz, C. G.; Smolinsky, G., Eds.; Electrochemical Society: Pennington, 1985; p 227.
 - 190. Robinson, B.; Shivashankar, In *Plasma Processing*; Mathad, G. S.; Schwartz, C. G.; Smolinsky, G., Eds.; Electrochemical Society: Pennington, 1985; p 206.
 - 191. Fujima, S.; Yano, H. *Electrochem. Soc. Ext. Abst.* **1986**, *86-2*, 456; *J. Electrochem. Soc.* **1988**, *135*, 1195.
 - 192. Melliar-Smith, C. M.; Mogab, C. J. In *Thin Film Processes*; Vossen, J. L.; Kern, W., Eds.; Academic: New York, 1978; p 497.
 - 193. Robb, F. *Semicond. Int.* **1979**, *2*(1), 60.
 - 194. Dieleman, J.; Sanders, F. H. M. *Solid State Technol.* **1984**, *274*, 191.
 - 195. a. Tu, Y. Y.; Chuang, T. J.; Winters, H. F. *Phys. Rev. B* **1981**, *23*, 23. b. Gerlach-Meyer, U.; Coburn, J. W.; Kay, E. *Surf. Sci.* **1981**, *103*, 177. c. Coburn, J. W. *Solid State Technol.* **1984**, *294*, 117.
 - 196. Donnelly, V. M.; Flamm, D. L.; Bruce, R. H. *J. Appl. Phys.* **1985**, *58*, 2135.
 - 197. Adams, A. C.; Capio, C. D. *J. Electrochem. Soc.* **1981**, *128*, 366.
 - 198. Zarowin, C. B. *J. Vac. Sci. Technol., A* **1984**, *2*, 1537.
 - 199. Chapman, B. N. *Glow Discharge Processes*; Wiley: New York, 1980; pp 299–305.
 - 200. Hirose, M. In *Semiconductors and Semimetals*; Pankove, J. I., Ed.; Academic: New York 1984; Vol. 21A, p 9.
 - 201. Hess, D. W. In *Reduced Temperature Processing for VLSI*; Reif, R.; Srinivasan, G. R., Eds.; Electrochemical Society: Pennington, 1986; p 3.
 - 202. Adams, A. C. In *Reduced Temperature Processing for VLSI*; Reif, R.; Srinivasan, G. R., Eds.; Electrochemical Society: Pennington, 1986; p 111.
 - 203. Nguyen, S. V. *J. Vac. Sci. Technol., B* **1986**, *4*, 1159
 - 204. Stuke, J. *Annu. Rev. Mat. Sci.* **1985**, *15*, 79.
 - 205. Kampas, F. J. In *Semiconductors and Semimetals*; Pankove, J. I., Ed.; Academic: New York 1984; Vol. 21A, p 153.
 - 206. Longeway, P. A. In *Semiconductors and Semimetals*; Pankove, J. I., Ed.; Academic: New York 1984; Vol. 21A, p 179.
 - 207. Reimer, J. A. In *Plasma Processing*; Coburn, J. W.; Gottscho, R. A.; Hess, D. W., Eds.; Materials Research Society: Pittsburgh, 1986; Vol. 68, p. 157.
 - 208. Zanzucchi, P. J. In *Semiconductors and Semimetals*; Pankove, J. I., Ed.; Academic: New York, 1984; Vol. 21B, p 113.
 - 209. Reimer, J. A.; Vaughan, R. W.; Knights, J. C. *Phys. Rev. Lett.* **1980**, *44*, 193; *Phys. Rev. B* **1981**, *124*, 3360.
 - 210. Harbison, J. P. *J. Non-Cryst. Solids* **1984**, *66*, 87.
 - 211. Roth, R. M.; Spears, K. G.; Stein, G. D.; Wong, G. *Appl. Phys. Lett.* **1985**, *46*, 253.

212. Spears, K. G.; Robinson, T. J. In *Plasma Processing*; Coburn, J. W.; Gottscho, R. A.; Hess, D. W., Eds.; Materials Research Society: Pittsburgh 1986, 68, 121.
213. Kamins, T. I.; Chiang, K. L. *J. Electrochem. Soc.* 1982, 129, 2326.
214. Townsend, W. G.; Uddin, M. E. *Solid-State Electron.* 1963, 16, 39.
215. Suzuki, S.; Itoh, T. *J. Appl. Phys.* 1983, 54, 1466.
216. Donahue, T. J.; Burger, W. R.; Reif, R. *Appl. Phys. Lett.* 1984, 44, 346.
217. Lanford, W. A.; Rand, M. J. *J. Appl. Phys.* 1978, 49, 2473.
218. Stein, H. J.; Wells, V. A.; Hampy, R. E. *J. Electrochem. Soc.* 1979, 126, 1750.
219. Chow, R.; Landford, W. A.; Ke-Ming, W.; Rosler, R. S. *J. Appl. Phys.* 1982, 53, 5630.
220. Paduscheck, P.; Hopfl, C.; Mitlehner, H. *Thin Solid Films* 1983, 110, 291.
221. Claassen, W. A. P.; Valkenburg, W. G. J. N.; Willemse, M. F. C.; Wijert, W. M. v. d. *J. Electrochem. Soc.* 1985, 132, 893.
222. Maeda, M.; Nakamura, H. *J. Appl. Phys.* 1985, 58, 484.
223. Knolle, W. R.; Osenbach, J. W. *J. Appl. Phys.* 1985, 58, 1248.
224. Samuelson, G.; Mar, K. M. *J. Electrochem. Soc.* 1982, 129, 1773.
225. Sun, R. C.; Clemens, J. T.; Nelson, J. T. In *Proc. IEEE Rel. Phys. Symps.*; 1980; p 244.
226. Fair, R. B.; Sun, R. C. *IEEE Trans. Electron Devices* 1981, ED-28, 83.
227. Dun, W.; Pan, P.; White, F. R.; Douse, R. W. *J. Electrochem. Soc.* 1981, 128, 1555.
228. Maeda, M.; Arita, Y. *J. Appl. Phys.* 1982, 53, 6852.
229. Katoh, K.; Yasui, M.; Watanabe, H. *Jpn. J. Appl. Phys.* 1983, 22, L321.
230. Cheng, H. S.; Zhou, Z. Y.; Yang, F. C.; Xu, Z. W.; Ren, Y. H. *Nucl. Instrum. Methods Phys. Res.* 1983, 218, 601.
231. Watanabe, H.; Katoh K.; Yasui, M. *Jpn. J. Appl. Phys.* 1984, 21, 1.
232. Reinberg, A. R. *Annu. Rev. Mat. Sci.* 1979, 9, 341.
233. Fujita, S.; Toyoshima, H.; Ohsishi, T.; Sasaki, A. *Jpn. J. Appl. Phys.* 1984, 23, L144; 23, L268.
234. a. Livengood, R. E.; Hess, D. W. *Appl. Phys. Lett.* 1987, 50, 560. b. Flamm, D. L.; Chang, C.-P.; Ibbotson, D. E.; Mucha, J. A. *Solid State Technol.* 1987, 30, 43.
235. Livengood, R. E.; Petrich, M. A.; Hess, D. W.; Reimer, J. A. *J. Appl. Phys.* 1988, 63, 2651.
236. Sinha, A. K.; Levinstein, H. J.; Smith, T. E.; Quintana, G.; Haszako, S. E. *J. Electrochem. Soc.* 1978, 125, 601.
237. Koyama, K.; Takasaki, K.; Maeda, M.; Takgi, M. In *Plasma Processing*; Dieleman, J.; Freiser, R. G.; Mathad, G. S., Eds.; Electrochemical Society: Pennington, 1982; p 478.
238. van de Ven, E. P. G. T. *Solid State Technol.* 1981, 244, 167.
239. Hollahan, J. R. *J. Electrochem. Soc.* 1974, 126, 930.
240. Reinberg, A. R. *J. Electron. Mat.* 1979, 8, 345.
241. Adams, A. C. *Solid State Technol.* 1983, 264, 135.
242. Goreczyca, T. B.; Gorowitz, B. In *VLSI Electronics: Microstructure Science*; Einspruch, N. G.; Brown, D. M., Eds.; Academic: New York, 1984; Vol. 8, p 69.
243. Adams, A. C.; Alexander, F. B.; Capio, C. D.; Smith, T. E. *J. Electrochem. Soc.* 1981, 128, 1545.
244. Smith, G. C.; Purdes, A. J. *J. Electrochem. Soc.* 1985, 132, 2721.
245. a. Tang, C. C.; Hess, D. W. *Appl. Phys. Lett.* 1984, 45, 633. b. Greene, W. M.; Oldham, W. G.; Hess, D. W. *Appl. Phys. Lett.* 1988, 52, 1133.
246. Hess, D. W. In *VLSI Electronics: Microstructure Science*; Einspruch, N. G.; Brown, D. M., Eds.; Academic: New York, 1984; Vol. 8, p 55.

247. Tang, C. C.; Chu, J. K.; Hess, D. W. *Solid State Technol.* **1983**, *263*, 125.
248. Tabuchi, A.; Inoue, S.; Maeda, M.; Takagi, M. *Jpn. Semicond. Technol. News*, **1983**, February, 43.
249. Akimoto, K.; Watanabe, K. *Appl. Phys. Lett.* **1981**, *39*, 445.
250. Rosler, R. S.; Engle, G. M. *J. Vac. Sci. Technol., B* **1984**, *2*, 733.
251. Kemper, M. J. H.; Koo, S. W.; Huizinga, F. *Electrochem. Soc. Ext. Abstracts*; New Orleans, October 7–12, 1984; Abst. No. 377.
252. Hieber, K.; Stoltz, M.; Wieczorek, In *Proceedings, Ninth International Conference on CVD*; Robinson, M.; Cullen, G. W.; van den Brekel, C. H. J.; Blocker, J. M., Jr.; Rai-Choudhury, P., Eds.; Electrochemical Society: Pennington, 1979; p 205.
253. Gleason, E. F.; Hess, D. W. In *Plasma Processing*; Coburn, J. W.; Gottscho, R. A.; Hess, D. W., Eds.; Materials Research Society: Pittsburgh, 1986; Vol. 68, p 343.
254. Williams, L. M. *Appl. Phys. Lett.* **1985**, *46*, 43.
255. Natarajan, V.; Lamb, J. D.; Woollam, J. A.; Liu, D. C.; Gulino, D. A. *J. Vac. Sci. Technol., A* **1985**, *3*, 681.
256. Warner, J. D.; Pouch, J. J.; Alterovitz, S. A.; Liu, D. C.; Landford, W. A. *J. Vac. Sci. Technol., A* **1985**, *3*, 900.
257. Meyerson, B. S. In *Plasma Processing*; Coburn, J. W.; Gottscho, R. A.; Hess, D. W., Eds.; Materials Research Society: Pittsburgh, 1986; Vol. 68, p 191.
258. Park, S. C.; Bodart, J. R.; Han, He.-X.; Feldman, B. J. In *Plasma Processing*; Coburn, J. W.; Gottscho, R. A.; Hess, D. W., Eds.; Materials Research Society: Pittsburgh, 1986; Vol. 68, p 199.
259. Wagner, J.; Wild, Ch.; Bubenzer, A.; Koidl, P. In *Plasma Processing*; Coburn, J. W.; Gottscho, R. A.; Hess, D. W., Eds.; Materials Research Society: Pittsburgh, 1986; Vol. 68, p 205.
260. Pouch, J. J.; Alterovitz, S. A.; Warner, J. D. In *Plasma Processing*; Coburn, J. W.; Gottscho, R. A.; Hess, D. W., Eds.; Materials Research Society: Pittsburgh, 1986; Vol. 68, p 211.
261. Fedoseev, D. V.; Varnin, V. P.; Deryagin, B. V. *Russ. Chem. Rev.* **1984**, *53*, 435.
262. Fujimori, N.; Imai, T.; Doi, A. *Vacuum* **1986**, *36*, 99.
263. Robinson, A. L. *Science (Washington, D.C.)* **1986**, *234*, 1074.

RECEIVED for review December 30, 1987. ACCEPTED revised manuscript October 27, 1988.